

## A LARGE-AREA SEARCH FOR LOW-MASS OBJECTS IN UPPER SCORPIUS II: AGE AND MASS DISTRIBUTIONS

CATHERINE L. SLESNICK\*, LYNNE A. HILLENBRAND & JOHN M. CARPENTER  
Dept. of Astronomy, MC105-24, California Institute of Technology, Pasadena, CA 91125  
*Draft version October 29, 2018*

### ABSTRACT

We present continued results from a wide-field,  $\sim 150$  deg<sup>2</sup>, optical photometric and spectroscopic survey of the northern part of the  $\sim 5$  Myr-old Upper Scorpius OB Association. Photometry and spectral types were used to derive effective temperatures and luminosities and place newly identified association members onto a theoretical Hertzsprung-Russell diagram. From our survey, we have discovered 145 new low mass members of the association, and determined  $\sim 10\%$  of these objects to be actively accreting material from a surrounding circumstellar disk. Based on comparison of the spatial distributions of low and high mass association members, we find no evidence for spatial segregation by mass within the northern portion of the association. Measured data are combined with pre-main sequence evolutionary models to derive a mass and age for each star. Using Monte Carlo simulations we show that, taking into account known observational uncertainties, the observed age dispersion for the low mass population in USco is consistent with all stars forming in a single burst  $\sim 5$  Myr ago, and place an upper limit of  $\pm 3$  Myr on the age spread if the star formation rate has been constant in time. We derive the first spectroscopic mass function for USco that extends into the substellar regime, and compare these results to those for three other young clusters and associations.

*Subject headings:* open clusters and associations: individual (Upper Scorpius) — stars: low-mass, brown dwarfs — stars: pre-main sequence — stars: mass function — stars: ages

### 1. INTRODUCTION

The review of Shu et al. (1987) laid the basic framework for how isolated stars are created. However, most stars do not form in isolation but rather in groups (i.e., clusters or associations; Gomez et al. 1993, Lada & Lada 1995, Carpenter 2000), and many details of the processes involved in stellar group formation remain unexplained. In particular, do all members of an individual group form in a single burst, or is star formation a lengthy process? The distribution of stellar masses formed within a stellar group is known as the initial mass function (IMF). Is the IMF universal, or does it vary with either star formation environment or time?

The phenomenon of rapid (1–2 Myr) clustered star-formation has been found in almost all nearby young associations (e.g., Lada & Lada 2003). The large numbers of very young stars and apparent lack of more evolved (5–10 Myr-old) objects in star forming regions contrasts with ages of a few tens of megayears (e.g., Blitz & Shu 1980) inferred for molecular clouds. Either star-formation takes place for only a small fraction of the cloud lifetime, molecular clouds themselves live only a few megayears (e.g., Hartmann et al. 2001), or older group members have been missed in observational surveys which are often biased towards stars that are still actively accreting or which possess an optically thick disk. Observational surveys capable of detecting the entire age range present within a stellar group are needed if we are to begin to understand the time dependence of star formation within a molecular cloud.

The basic structure of the field star IMF in the mass

range  $\sim 0.5 M_{\odot}$  to  $10 M_{\odot}$  is well characterized by a power law with slope  $dN/dM \propto M^{-2.35}$ , as derived originally by Salpeter (1955). However, while the shape of the stellar mass function between  $\sim 0.5 M_{\odot}$  and  $10 M_{\odot}$  is near universal, below  $\sim 0.5 M_{\odot}$  the shape of the mass function may be strongly dependent on environment within the parental molecular cloud (Luhman et al. 2003b, Slesnick et al. 2004). Young stellar clusters and associations are particularly valuable for examining the shape of the low mass IMF because contracting low-mass pre-main sequence stars and brown dwarfs are 2–3.5 orders of magnitude more luminous than their counterparts on the main sequence. Thus, despite the fact that they are farther away, young stars and brown dwarfs can be more readily detected than stars of equivalent mass in the field.

The Upper Scorpius OB Association (USco) is the closest (145 pc; de Zeeuw et al. 1999) young OB association to the Sun with 120 members more massive than  $\sim 1 M_{\odot}$ , and an associated population of  $\sim 400$  known low mass objects (e.g., Preibisch et al. 1998). Because of its proximity, and large population that spans the range from  $< 0.02 M_{\odot}$  to  $> 10 M_{\odot}$ , USco is an ideal region in which to study the mass distribution of stars in OB associations. Furthermore, at an age of  $\sim 5$  Myr (Preibisch et al. 2002), USco is young enough that we may be able to measure the ages of member stars to a precision of less than a million years, and old enough that an on-going episode of star formation lasting several millions of years could be detectable. A major difficulty faced by studies of the USco region is that the high mass members alone span  $> 300$  deg<sup>2</sup> on the sky. Obtaining a complete census of the association's low mass population is thus a formidable task as one must identify faint objects over a very large spatial region. While there exist several techniques to

\*current address: Dept. of Terrestrial Magnetism, Carnegie Inst. of Washington, Washington, DC 20015  
Electronic address: cslesnick@ciw.edu, lah@astro.caltech.edu, jmc@astro.caltech.edu

identify young stars, many observational signatures (e.g.,  $H\alpha$  emission or near-infrared excess) probe accretion processes and circumstellar material rather than characteristics intrinsic to the stars themselves.

Recently, deep, multicolor imaging surveys combined with spectroscopic follow-up have proven successful in identifying low mass stars and brown dwarfs without active accretion, as well as classical T-Tauri type objects. Young pre-main sequence (PMS) objects still undergoing contraction are cooler (i.e., redder in color) and/or more luminous (i.e., brighter in magnitude) than their main sequence counterparts. In nearby regions, candidate PMS stars can be identified through photometric colors and magnitudes that are systematically different from those of the bulk field star population. Spectroscopic follow-up observations allow assessment of surface gravity diagnostics which can be used to distinguish bonafide young PMS stars from foreground field dwarfs and reddened background giants. Previous imaging and spectroscopic surveys in USco include studies by Preibisch et al. (2001) and Preibisch et al. (2002), whose work yielded 166 new low mass PMS objects. Lodieu et al. (2008), Martín et al. (2004), and Ardila et al. (2000) together identified  $\sim 70$  members of USco with spectral type M6 or later. Thus far, over 400 low mass ( $M < 0.6 M_{\odot}$ ) members have been identified in USco through X-rays,  $H\alpha$  emission, photometry and/or spectroscopy. However, most searches have been limited to small subregions (smaller than a few square degrees) or bright objects ( $R \lesssim 16$  mag). Given the derived mass function and number of observed high mass stars in USco, and assuming the high and low mass objects share the same spatial distribution, Preibisch et al. (2002) estimate the entire USco region should contain  $>1500$  young, low mass objects with  $M < 0.6 M_{\odot}$ , most of which are yet to be discovered.

In Slesnick, Carpenter, & Hillenbrand (2006a; hereafter Paper I), we introduced our wide-field photometric survey covering  $\sim 150$  deg<sup>2</sup> of USco. In that work, we presented optical spectroscopic observations of 62 photometrically-selected candidate PMS stars, of which 43 were confirmed by us to be new USco members. In this companion paper we present spectra for an additional 178 candidates observed at either Palomar Observatory or Cerro-Tololo Inter-American Observatory (CTIO). In §2, we give a brief overview of the photometric and spectroscopic surveys, and present new USco members discovered as a result of recent observations. For the remainder of the paper beyond §2, we discuss results for new members presented here together with those for association members identified in Paper I. In §3, we discuss  $H\alpha$  emission profiles and accretion signatures in USco. In §4, we compare the spatial distribution of the high and low mass populations. Finally, in §5, we construct an Hertzsprung-Russell (HR) diagram and present a discussion of the age and mass distributions derived for the members of USco presented in our work, as well as a comparison of distributions derived for other nearby star forming regions.

## 2. OBSERVATIONS

### 2.1. *Quest-2 Photometric Observations and Candidate Member Selection*

Driftscan observations were taken with the Quest-2 camera (Rabinowitz et al. 2003, Baltay et al. 2007) on the 48-inch (1.2-m) Samuel Oschin Schmidt Telescope at Palomar Observatory. Details of the observations and data analysis are given in Paper I, Slesnick, et al. (2006b; hereafter SCH06), and Slesnick (2007). Three  $4.6^{\circ}$  wide scans, centered at  $\delta = -15.7^{\circ}$ ,  $-19.5^{\circ}$ , and  $-23.3^{\circ}$ , were each observed between R.A. of 15h46m and 16h36m for a total survey area of  $\sim 150$  deg<sup>2</sup>. The scan centered at  $\delta = -19.5^{\circ}$  was observed 3–4 times per night on seven consecutive, photometric nights between 2004 June 20–26. The other two scans were observed once during this period.

$B, R, I$  photometric data were calibrated to a system closely aligned with *Sloan*  $g, r, i$  magnitudes as described in SCH06 and Slesnick (2007). Magnitudes for all the new USco members identified in this study (based on a combination of photometry and spectroscopy; see §2.4), both those newly identified in this work and those identified originally in Paper I, are given in Table 1. Our goal is to use the photometry to isolate PMS stars from the field star population which dominates the  $\sim 2$  million member source catalog. As discussed in §1, nearby young stars occupy a sequence in an optical color-magnitude diagram (CMD) that is systematically brighter and/or redder than the sequence occupied by most field stars, and thus can be identified based on their colors and magnitudes. While the data have been calibrated to approximate *Sloan* magnitudes [see Slesnick (2007) for more details], they are not precisely on any standard system, and we did not translate theoretical isochrones into the Quest-2 system. Thus, we did not select candidates based on isochronal data and instead, considered as candidate PMS stars all sources redward of a linear approximation of the 1% data contour in an  $r, r - i$  CMD (Figure 1). This criterion roughly corresponds to selecting all candidates redward of a 30 Myr isochrone.

In addition to optical colors, the infrared colors and magnitudes of potential PMS candidates were also considered. We matched the entire source catalog to the 2 Micron All Sky Survey (2MASS; Skrutskie et al. 2006) and excluded from further consideration sources which did not have a 2MASS counterpart. This criteria served to remove artifacts detected in the 2 driftscans for which we did not have repeated observations. However, as discussed in Paper I and SCH06, requiring a 2MASS detection biases the list of potential PMS candidates against faint blue sources. The position of each star on a near-infrared color-color diagram was examined and any star with  $J - H, H - K_S$  colors consistent with those of background giants [ $(J - H) > 0.6(H - K_S) + 0.6$  or  $(J - H) > 1.69(H - K_S) + 0.29$ ]; Bessell & Brett (1988)] was excluded. We additionally considered  $r - K_S$  colors and adopted the selection criterion  $r < 2.57(r - K_S - 3) + 12.8$  as outlined in Paper I. After all selection criteria were applied, the final candidate list contained  $\sim 1700$  candidate low mass PMS stars identified from  $\sim 2$  million sources detected in the Quest-2 survey. Of these stars, 90 correspond to previously known low mass members of USco (Ardila et al. 2000, Preibisch et al. 2002, Martín et al. 2004). The candidates were spread out over the entire  $\sim 150$  deg<sup>2</sup> survey area, which encompasses  $\sim 40\%$  of the total spatial area spanned by the high mass members. Due to interstellar extinction and distance effects, op-

tical and near-infrared colors and magnitudes alone are not a unique indicator of youth. Therefore, it is necessary to obtain spectroscopic follow-up observations for each photometrically-selected candidate. This data allows for spectral type determination and can confirm the presence of spectral features indicative of youth.

### 2.2. Palomar Spectroscopy

Moderate-resolution spectra of 105 PMS star candidates were taken with the Double Spectrograph on the Palomar 200-inch telescope during the nights of 2006 May 16–19 and 2006 June 1–2. All data were taken with the red side of the spectrograph through either the 1.5” or the 2” slit using a 5500 Å dichroic and a 316 lines  $\text{mm}^{-1}$  grating blazed at 7500 Å. This set-up produced wavelength coverage from 6300 to 8825 Å at a resolution of  $R \sim 1250$ . Typical exposure times were 300–900 sec, and up to 1800 sec for the faintest targets ( $r \sim 20$ ). Spectrophotometric standard stars (Massey et al. 1988) were observed throughout each night for flux calibration. All sources were processed, extracted and calibrated using standard IRAF tasks.

Spectral analysis for these observations were carried out as detailed in Paper I, SCH06, and Slesnick (2007). Both spectral type (temperature) and surface gravity (age) determinations were first made through quantitative measurements of the TiO-7140, TiO-8465, and Na-8190 indices (defined in Paper I) which measure the strength of molecular and atomic absorption features present at optical wavelengths in the spectra of K- and M-type stars. Figure 2 shows spectral indices for 167 PMS spectral candidates in the USco region observed at Palomar (105 presented here for the first time and 62 presented in Paper I). The left panel shows measurements of temperature-sensitive indices used to aid in spectral type determination. We find fourteen outliers sit below the main locus of data points. In all cases, the star is confirmed to exhibit low gravity signatures (see below) and we attribute the position in Figure 2 to a small amount of veiling or reddening. A detailed explanation of the possible effects of these processes on the classification indices is given in Paper I and SCH06.

The surface gravity-sensitive Na-8190 index (Figure 2, right panel) allows us to easily separate the bona fide low gravity (i.e., young) objects from contaminant dwarf stars over the spectral-type range  $\sim M3$ – $M8$ . We find a large fraction ( $\sim 65\%$ ) of the candidate objects have measured Na-8190 indices consistent with their having surface gravity less than that of field dwarfs at similar spectral types. The TiO and Na quantitative spectral indices were used to aid in classification only. All final spectral type and gravity determination were done by visually comparing each spectrum to a grid of spectral standard stars observed throughout the observing run.

### 2.3. Cerro Tololo Spectroscopy

Additional spectra of PMS star candidates in USco were taken at CTIO using the Hydra multifiber spectrograph on the Blanco 4-m telescope during the nights of 2005 July 24–28. In total, 26 pointings were observed with the Site 2k $\times$ 4k CCD through the KPGLF grating. The setup provided wavelength coverage from  $\sim 6300$  to 8660 Å at a resolution of 1.15 Å/pixel.

Fibers were placed preferentially on stars meeting the criteria outlined in §2.1, thus providing a sample of candidates analogous to those observed at Palomar. Remaining fibers were placed on stars meeting one or more of the criteria outlined in §2.1. For the practical requirements of the Hydra observations, stars were assigned to either ‘bright’ pointings (corresponding to  $r \lesssim 16.5$ ) or ‘faint’ pointings (corresponding to  $16.5 \lesssim r \lesssim 18.5$ ). Exposure times ranged from 900 to 1800 sec for bright pointings (dependent on weather conditions), and were set at 2700 sec for faint pointings. In total, 10 bright and 16 faint pointings were observed during the 5 nights. At each fiber configuration, we observed spectra of a comparison lamp and a quartz lamp to allow determination of the dispersion solution and throughput correction during data reduction. Biases and dome flats were taken each afternoon with all working fibers put in the ‘large circle’ configuration. Milk flats (see below) were taken once during the observing run.

#### 2.3.1. Image Processing and Sky Subtraction

All frames were first pre-processed (bias correction and trimming) in IRAF using the CCDPROC task. Milk flats were obtained on the second afternoon of observing. This type of observation is an exposure of the daytime sky, and is taken through a plate of milky glass placed between the output of the fibers and the spectrograph camera. The purpose of milk flats is to allow removal of CCD pixel-to-pixel variations from the data in the absence of fibers. After median-combining all observed milk flats, a spectral response image was created by smoothing in both X and Y directions. The original combined milk flat was divided by the spectral response image to create an image with a value of 1.0 everywhere except where pixel-to-pixel variations exist. All data and calibration frames were divided by this image.

Subsequent data reduction was done using the IRAF dohydra task. All data for a given night were divided by the dome flat taken that afternoon. Individual fiber-to-fiber throughput corrections (which change for each configuration) were made from division of each object frame by the corresponding quartz lamp spectra taken in the same fiber configuration. Wavelength calibration was carried out by matching each object spectrum to the corresponding lamp spectrum observed through the same fiber.

For each pointing, a single sky spectrum was made using the sky generating tasks within dohydra. Typically,  $\sim 5$ – $20$  fibers were placed on sky during each observation. The dohydra sky generating task first allows rejection of any anomalous sky spectra which may have inadvertently fallen on a star or a clump of nebulosity. Remaining sky spectra are averaged together using a  $3\sigma$  clipping algorithm. The hydra field of view is 40’ on a side. We found subtraction of a single sky spectrum for all spectra within a field often produced insufficient sky subtraction in that, for a given spectrum, all sky lines could be systematically over- or under-subtracted. To correct this problem, for each spectrum we computed the flux in a single sky line chosen to be towards the center of the spectrum ( $\sim 7316$  Å) and to be sufficiently isolated that it was not blended with any other sky or stellar lines. Object spectra were scaled such that the flux computed in the central sky line matched that of the sky spectrum

and the sky spectrum was subsequently subtracted.

### 2.3.2. Classification

Spectral observations taken through fibers produce flux that varies as a function of wavelength, dependent on the fiber configuration (i.e., how the relevant fiber is bent and stretched to place it into position on the star). Thus, flux correction of fiber data is inherently difficult because it is not practical to observe a calibrator star through every fiber at every configuration. We were therefore not able to flux-correct the hydra spectra in a manner analogous to the Palomar data and could not use the quantitative spectral indices (which rely on flux-corrected spectra) to aid in classification. Though the overall spectral shape is not meaningful because the spectra are not flux corrected, the depth of absorption and emission features is not substantially affected. During observations, we observed a range of known dwarf and giant stars (spectral types K0–M8). In addition, we observed known intermediate-age PMS members of the  $\sim 30$  Myr-old Tucanae Hor association (Mamajek et al. 2004) with early M spectral types. Spectra of previously identified K0–M8-type USco members were observed in pointings towards USco along with program candidates. All spectra of candidate PMS stars were classified by hand through comparison to each other and to standard stars observed with hydra.

In total, the hydra observations yielded  $\sim 1150$  spectra (of varying quality). We first classified all of the spectra into broad categories. Approximately 450 were determined to be mid K to M ‘late-type’ stars based on the presence of TiO molecular absorption in their spectra, and a lack of  $H\alpha$  absorption. The largest constituent of the spectral sample ( $\sim 650$  stars) were ‘mid-type’ stars with spectral types late F through early K. These stars are characterized by a lack of TiO molecular absorption but the presence of Ca II triplet ( $\lambda 8498$ ,  $\lambda 8542$ ,  $\lambda 8662$  Å) and  $H\alpha$  atomic absorption. Absorption from the Ba II, Fe I, Ca I blend at  $\lambda 6497$  Å begins to appear at late F/early G types and increases in strength compared to  $H\alpha$  absorption through K spectral types. Thirty of the late F – early K type stars have  $H\alpha$  emission present in their spectra. The remaining  $\sim 50$  stars observed with hydra were determined to have spectral types A–F with deep  $H\alpha$  and Ca II triplet absorption but noticeably lacking any absorption at the  $\lambda 6497$  Å blend. As expected, we saw no evidence of He absorption in any of the spectra and conclude that our survey did not probe B- or O-type stars.

Magnitude histograms for the samples of observed ‘mid-type’ and ‘late-type’ stars are shown at  $r$ - and  $J$ -band (Figure 3), along with the range of magnitudes expected for members of USco at these spectral types. We have assumed for this calculation that all members of USco are 5 Myr-old, 145 pc away, and have  $0 \leq A_V \leq 2$  (Paper I). As can be seen, most of the stars classified as mid-type do not appear to be members of USco based on their observed magnitudes and spectral types. This sample is instead likely dominated by reddened field dwarfs and background giants. This result is not surprising, considering most of these stars were observed through fibers placed on stars in the field of view that did not meet all 3 criteria for candidate selection (see §2.3 and §2.1), and

were not part of the  $\sim 1700$ -member candidate list.

Thus far, we have derived detailed (at the  $\sim 0.5$  subclass level) classifications from these data only for those stars whose colors and magnitudes meet all of the selection criteria outlined in Paper I and SCH06, thus providing a sample selected in exactly the same manner as the stars observed at Palomar. This sample was determined to consist entirely of late K- and M-type stars,  $\sim 50\%$  of which have low surface gravity consistent with association membership. We present here results for these stars together with results from the Palomar spectral observations.

### 2.4. Summary of Observations

We identified a total of  $\sim 2$  million sources in the  $\sim 150$  deg<sup>2</sup> area covered by the Quest-2 imaging survey of the northern part of USco. The survey encompassed 56 out of 120 high mass association members identified with Hipparcos (de Zeeuw et al. 1999), and  $\sim 40\%$  of the total spatial area spanned by the high mass members. Using a combination of Quest-2  $g, r, i$  and 2MASS  $J, H, K_S$  magnitudes, we selected  $\sim 1700$  candidate young stars based on placement in color-color and color-magnitude diagrams. Specifically, to be considered as a candidate PMS star, the object was required to be within the reddest 1% (in  $r - i$  color) of stars observed in our survey, and to have infrared colors inconsistent with field giants.

We obtained optical spectra for  $\sim 15\%$  of the photometric candidates selected to be among the reddest of the photometric candidates across all magnitudes ( $14 \lesssim r \lesssim 20$ ) probed. The goal of the spectroscopic observations is to measure spectral type and confirm low gravity signatures consistent with bona fide PMS stars for each photometric candidate. From the 105 Palomar spectral observations presented here (§2.2), we identified 66 new USco members with spectral types ranging from M3 to M8. We present an additional 36 new members with spectral types M3–M8 identified from CTIO observations. Quest-2 and 2MASS magnitudes for photometric candidates determined spectroscopically to be field dwarfs are given in Table 3.

For the remainder of this paper, we will discuss together results from both the 102 new low mass USco members presented here, and the 43 members presented in Paper I. Magnitudes and spectral measurements (i.e., spectral type,  $H\alpha$  equivalent width, and spectral indices, when applicable) for the 145 members identified by us are given in Table 1. Together, these stars represent a uniformly selected sample of new low mass USco members that is free from bias in regards to circumstellar material and activity.

## 3. EMISSION LINE OBJECTS

The most prominent emission line observed in the spectra of new members is  $H\alpha$  which, seen in the spectra of young stars and brown dwarfs, is created via one of several mechanisms. Weak, narrow  $H\alpha$  lines are presumed to originate from active chromospheres whereas strong, broad and/or asymmetric lines can be produced from high-velocity, infalling accretion or strong winds. Barrado y Navascués & Martín (2003) have proposed an empirical, spectral type- $H\alpha$  equivalent width ( $W(H\alpha)$ ) relation to describe the upper limit of non-accreting stars and brown dwarfs based on the chromospheric saturation

tion limit observed in the Pleiades,  $\alpha$  Per, and IC 2391 open clusters. These clusters are sufficiently old (50–125 Myr) that accretion should not be present, and any observed H $\alpha$  emission is assumed to be produced entirely from chromospheric activity. Figure 4 plots measured H $\alpha$  equivalent widths as a function of spectral type for the 145 members of USco presented here, shown with the Barrado y Navascués & Martín (2003) empirical accretor/nonaccretor division. Notably, every new member identified in our work shows H $\alpha$  in emission. Many stars and brown dwarfs exhibit very strong H $\alpha$  emission (see also Table 1) at levels substantially above the accretor/nonaccretor division, and thus are possibly still undergoing active accretion.

We determined an empirical criterion for identifying objects with H $\alpha$  excess emission based on our data. At an age of  $\sim 5$  Myr, we assume the bulk of our sample is no longer accreting and compute median values of H $\alpha$  emission as a function of spectral type using 1-sigma clipping to remove any bias from outliers. For most bins, we define a star to have an H $\alpha$  excess if it exhibits emission at a level greater than  $3\sigma$  above the median value for its spectral type, where  $\sigma$  is the dispersion about the median for stars at a given spectral type. Stars with such strong H $\alpha$  emission are likely to be accreting and are assumed such for the remainder of this work. These sources are distinguished on Figure 4. For spectral type bins earlier than M4 and later than M7, we have identified fewer than 5 stars per spectral type. Thus, for these bins we do not have enough measurements to derive a statistically representative value for median H $\alpha$  emission and we do not consider any stars in these bins to be in our sample of H $\alpha$  excess, accreting sources. However, we note that two M8 stars (including the possible binary discussed in Paper I §4.2) sit above the Barrado y Navascués & Martín (2003) accretor/nonaccretor dividing line.

Based on the above criterion, we find 15 objects to exhibit H $\alpha$  emission with sufficient strength to be considered by us to be actively accreting. Spectra for accreting stars and brown dwarfs are shown in Figure 5. In addition to H $\alpha$  emission, many of these stars (SCH J16014156-21113855, SCH J16222156-22173094, SCH J16150524-24593542, SCH J16033470-18293060, SCH J16075565-24432714, SCH J16284706-24281413, SCH J16103876-18292353, SCH J16110739-22285027, SCH J16060391-20564497) also exhibit He I (6678 Å) emission which is commonly seen in spectra of classical T-Tauri type objects. Two accreting sources lie very close (within  $\sim 1^\circ$ ) to the young ( $\lesssim 1$  Myr)  $\rho$  Ophiuchi molecular cloud ( $\rho$ Oph;  $\alpha=16\ 25\ 35.118$ ,  $\delta=-23\ 26\ 49.84$  J2000). However, because  $\rho$  Oph lies slightly in front of USco (Loinard et al. 2008), if these stars were dynamically ejected  $\rho$  Oph members, we would expect to see them exhibit systematically higher luminosities than USco members of similar spectral type. Based on the derived HR diagram from these data (see §5.1) this phenomenon is not observed, and we include these two stars in our sample of accreting members of USco. We find at an age of  $\sim 5$  Myr (see §5.2), 15/145 (or  $\sim 10^{+3}_{-3}\%$ ) of low mass association members (spectral type  $\leq$  M7 and  $\geq$  M4) are observed to be accreting based on the strength of H $\alpha$  emission present in their spectra. If we were to use the Barrado y Navascués & Martín (2003)

accretion boundary instead of our own empirical classification, we would have determined 23/145 (16%) low mass stars and brown dwarfs in our sample are still accreting. In comparison, Guieu et al. (2006) find  $\sim 65\%$  (20/31) of 1 Myr-old low mass objects in the subclusters of Taurus to be actively accreting based on the strength of H $\alpha$  emission observed in their spectra compared to the Barrado y Navascués & Martín (2003) accretion boundary. Thus, a significant fraction of very low mass stars and brown dwarfs must stop accreting between 1 and 5 Myr. This conclusion is consistent with a median accretion lifetime of  $\sim 2$ – $3$  Myr for higher mass stars (Haisch et al. 2001, Hillenbrand 2005).

#### 4. SPATIAL DISTRIBUTION OF LOW MASS STARS

Figure 6 shows the 2D spatial distribution of the 120 high mass members of USco identified in the Hipparcos survey (de Zeeuw et al. 1999). This sample represents the complete population of known members more massive than  $\sim 1 M_\odot$ . The density of high mass stars is roughly constant from  $237^\circ \lesssim \alpha \lesssim 249^\circ$  and peaks at  $\delta \sim 24^\circ$ . As can be seen, despite the large area of the Quest-2 survey, it still encompassed only the central  $\sim 13^\circ$  in RA and the northern  $\sim 12^\circ$  in DEC of the association.

In general, the low mass PMS stars presented here share a common spatial distribution with the high mass Hipparcos members. Efforts to observe northwest of the Hipparcos stars largely yielded reddened field dwarfs rather than young association members. To correct for bias in the spatial area we observed spectroscopically, we first computed the percent of photometric candidates that we observed spectroscopically, in 1-degree bins, as a function of right ascension and declination. We found that we observed spectroscopically a maximum of  $\sim 25\%$  of the photometric candidates with a given degree-wide spatial bin. We thus corrected every bin to a uniform 25% of candidates observed, and calculated the number of members we would have detected assuming we had observed 25% of the photometric candidates in each bin, and that the percentage of identified members relative to the number of stars observed spectroscopically at each spatial bin would remain unchanged. Figure 7 shows the resultant 1D spatial distributions for the low mass association members discussed here, together with those for the 56 Hipparcos stars that fall within our survey area. We conclude that the density of low mass association members found in the Quest-2 survey is roughly uniform in RA, and peaks at  $\delta \sim -25^\circ$  with stellar densities falling off beyond these values. We find no evidence for spatial segregation by mass in USco within the northern portion of the association.

### 5. AGE AND MASS DISTRIBUTIONS

#### 5.1. HR Diagram for New USco Members

In this section, we combine the spectral type and photometry of each new member to derive values for its luminosity and effective temperature, and place it onto an HR diagram. As described in §2.1, the final Quest-2 photometry is not on a standard magnitude system. Thus, because of the reliability and uniformity of the 2MASS survey, we chose to use  $J$ -band magnitudes and  $(J - H)$  colors to derive luminosities. An empirical fit to  $BC_J$  as a function of spectral type was determined from the observational data of Leggett et al. (1996) and

Leggett et al. (2002) (spectral types M1-M6.5 and M6-L3, respectively). We derived intrinsic colors, extinction, and effective temperatures using the methods described in Slesnick et al. (2004).

In Figure 8, we present an HR diagram for the 145 low mass members of USco that we identified, shown with PMS model tracks and isochrones. The most commonly used PMS models for low mass stars and brown dwarfs are those derived by D’Antona & Mazzitelli (1997) (hereafter DM97) and Baraffe et al. (1998), which differ primarily in their atmospheric approximations and treatment of convection. Both models suggest similar mass ranges for our data of  $0.02M_{\odot} < M < 0.2M_{\odot}$ , though predicted masses for individual objects can vary by up to  $0.09M_{\odot}$  (60%). We have found that the slope of the DM97 isochrones provide a reasonable match to the derived HR diagram, whereas the Baraffe et al. (1998) models predict systematically younger stars at lower masses. A similar result was also noted by Hillenbrand et al. (2008). These authors compared the slope of six different theoretical PMS isochrones as a function of binary fraction, and found that, assuming an intermediate binary fraction consistent with observations (e.g., Kraus et al. 2008), the DM97 models provide the best match to the observed HR diagram slope for stars in USco. Thus, for the remainder of this work, we use the DM97 mass tracks and isochrones to derive mass and age for stars in our sample. All derived quantities are given in Table 2.

## 5.2. Age Distribution of the Low Mass Population in USco

Literal interpretation of the derived HR diagram (Figure 8) reveals a population with median age of  $\sim 4.1$  Myr, and a continuous spread of ages over  $\gtrsim 10$  Myr. While this result *may* be real, the continuous nature of the observed age distribution in USco could also be produced from uncertainties in observed parameters. Unlike the HR diagram, the observed surface gravity-sensitive spectral features do not show evidence for a large spread in age between association members. Figure 9 shows spectra of two stars with spectral type M5 identified in the survey. The top spectrum is that of the ‘youngest’ M5 star observed spectroscopically at Palomar (SCH16054416-21550566),  $\sim 2.6$  Myr-old based on its location on the HR diagram (see also Table 2); the bottom spectrum is of the ‘oldest’ M5 star observed at Palomar (SCH16162599-21122315),  $\sim 14.4$  Myr based on its location on the HR diagram. As discussed in SCH06 and Slesnick (2007), young stars less than a few megayears old exhibit systematically less Na I ( $\lambda 8190$  Å) absorption than do intermediate-age stars ( $\sim 5$ – $10$  Myr) due to their lower surface gravity (see Figure 10 in Paper I and Figure 6 in SCH06). Thus, if the derived ages from the HR diagram are correct, the spectrum of the 14.4 Myr-old star should have noticeably stronger Na I absorption. For example, an M5 star at 1–5 Myr would have a Na-8190 index 5–10% larger than that observed for an M5 star at 10 Myr. The spectra presented in Figure 9 are nearly identical (and have near-identical measured Na-8190 indices of 0.89 and 0.90). Based on analysis of spectral features, we classified these two stars as being roughly the same age. However, based on the differences in observed luminosity, interpreting the HR diagram lit-

erally, one would infer an age spread of  $>10$  Myr between the two stars.

### 5.2.1. Comparison of the Observed Age Distribution to a Coeval Population

Due to the discrepancy between stellar ages derived from the HR diagram compared to those inferred from spectral surface gravity signatures, we sought to determine the statistical significance of the observed spread in ages for stars on the HR diagram. Effective temperatures and luminosities shown in Figure 8 are derived from observed  $J$  magnitudes,  $J - H$  colors, and spectral types. The age and mass of a star are inferred from effective temperature and luminosity using a set of theoretical isochrones and mass tracks. Thus, uncertainties in measured photometry or spectral type are propagated into uncertainties in mass and age. Variations in distance and binarity can cause additional uncertainty in luminosity, and, hence, quantities derived from the HR diagram.

We explore first the possibility that the USco population could be coeval, and the apparent age spread in the HR diagram is a result of observational uncertainties combined with association depth and binarity effects. Using a similar method to that used in this work, Preibisch & Zinnecker (1999) compute an age of  $\sim 5$  Myr for the intermediate-mass members of USco. We used Monte Carlo techniques to generate a coeval population of 5 Myr-old stars and brown dwarfs at a distance of 145 pc. The input spectral type distribution was selected to mirror that of our observed distribution of stars, with 1000 stars simulated for every star observed. For each star in the simulated population,  $J$ - and  $H$ -band magnitudes were varied by adding random offsets drawn from a Gaussian distribution with a 1-sigma deviation of 0.025 mag, corresponding to the average uncertainty in the 2MASS photometry for observed stars. To mimic the magnitude-limited data sample, we did not allow any star to be simulated below the photometric survey limits ( $J=16$  and  $H=15.5$ ). Similarly, a random offset was added to the assumed spectral type, selected from a Gaussian distribution with 1-sigma errors of 0.5 spectral subtypes corresponding to the qualitative error of the optical spectral type determinations. Simulated spectral types were rounded to the nearest 0.25 subclasses to reflect the discreet nature of spectral type classification for new members discovered in our work. Using the new spectral type, for each simulated star, we re-derived the expected effective temperature, bolometric correction and intrinsic  $J - H$  color using the methods described in Slesnick et al. (2004).

The maximum distance spread (derived from secular parallax measurements) among members of the association with Hipparcos measurements is 50 pc (Preibisch et al. 2002; de Bruijne 1999). In the simulation, we assumed a uniform spatial distribution over a box of this depth centered at 145 pc. A 33% binary fraction for stars across all simulated spectral types (M3–M8) was assumed, consistent with observational results of the binary frequency for low mass members of USco (Kraus et al. 2008, Kraus et al. 2005). All observed low mass binaries in USco have near equal masses ( $m_{\text{secondary}}/m_{\text{primary}} \gtrsim 0.6$ ; Kraus et al. 2005), and thus, the assumption was made that all binaries were

composed of two equal mass stars. This assumption is somewhat liberal in that it will produce the largest possible dispersion in luminosity.

We compare quantitatively results of this simulation to the observed data in Figure 10. The red shaded histogram shows the age distribution derived from the Monte Carlo simulation, overplotted with a histogram of ages for the data (black hatched histogram). Both histograms have been normalized to unity at the peak for comparison, and all stars with  $\log(T_{eff}) < 3.4$  (beyond which interpolation of the isochrones becomes unreliable) have been excluded from the data and the model results. The widths of the distributions are remarkably similar, given the simplistic nature of the Monte Carlo simulation. For the simulated association, we find a mean apparent age of  $\log(age)=6.51\pm 0.40$  whereas for the data (not including the 3 M8 stars) we find a mean age of  $\log(age)=6.53\pm 0.47$ . The data and the model differ significantly at the distribution tails, which is most likely caused either by an incorrect assumption of one of the model parameters, or by an inherent problem with the theoretical isochrones at very low masses (Hillenbrand & White 2004). To quantitatively assess how well the model reproduces the bulk of the data, excluding the distribution tails, we applied a  $\chi^2$  test of the central peaks of the distributions from  $\log(age)=6.0$  to  $\log(age)=7.4$ . This test yields a  $\sim 53\%$  probability that the two distributions could have been drawn from the same population. Thus, given the uncertainties, the data are consistent with most stars in USco forming via a single burst  $\sim 5$  Myr ago.

This result is somewhat surprising given the large extent of the association ( $\sim 35$  pc across). Assuming a sound speed of  $c_S=0.2$  km/s consistent with a  $T=10$  K molecular cloud, and assuming the stars formed close to where they are observed today, the sound crossing time for the parental molecular cloud is  $\sim 85$  Myr. Thus, one end of the cloud could not have ‘communicated’ to the other in time to create a simultaneous burst of star formation. This result does not, however, rule out the possibility that star formation happened simultaneously throughout the extent of the cloud because every part independently reached the threshold for star formation at the same time. Another scenario is that the stars formed much closer together and have since spread to their current positions. However, this possibility can be ruled out from simple arguments. The velocity dispersion of the massive Hipparcos members is  $\sim 1.3$  km/s (de Bruijne 1999). In 5 Myr, the furthest an association member could travel at a speed of 1.3 km/s is  $\sim 6.5$  pc, less than half the radius of the current association.

A similar discrepancy between a small observed age spread and the large spatial extent of the association has also been noted in the literature for USco’s intermediate and high mass members (Preibisch & Zinnecker 1999). To explain the disparity, Preibisch & Zinnecker (1999) (and later Preibisch & Zinnecker 2007) proposed a scenario in which star formation in USco was triggered by an external event in the form of a supernova explosion in the neighboring Upper Centaurus-Lupus association ( $\sim 70$  pc away and  $\sim 17$  Myr-old). They argue based on the structure and kinematics of large H I loops surrounding Sco Cen, that such an event is evidenced to have occurred  $\sim 12$  Myr ago. If true, the explosion would have driven

a shock wave that would have reached USco about  $\sim 5$  Myr ago, consistent with the inferred age of USco’s stellar population. Our results may imply a similar small age spread with an association age  $\sim 5$  Myr and large spatial extent (see §4) for USco’s lowest mass stars and substellar members. While our results do not prove the Preibisch & Zinnecker (1999) hypothesis true, they do give support to the hypothesis’ plausibility, and extend its validity to even the lowest mass association members.

### 5.2.2. Comparison of the Observed Age Distribution to a Uniform Distribution

From the simulation discussed in §5.2.1, we have determined the observed age distribution in USco is consistent with all stars forming in a single burst 5 Myr ago. We explore also the maximum age spread that can be inferred from our data assuming that the star formation rate has been constant in time. We repeated the original Monte Carlo simulation allowing age to vary in addition to spectral type, photometric error, distance and binarity. We began with a 5 Myr population, and for each star added a random offset in age drawn from a uniform population between  $\pm 0.5$  Myr,  $\pm 1$  Myr,  $\pm 1.5$  Myr,  $\pm 2$  Myr,  $\pm 2.5$  Myr,  $\pm 3$  Myr,  $\pm 3.5$  Myr,  $\pm 4$  Myr,  $\pm 4.5$  Myr, or  $\pm 5$  Myr. This age offset had the effect of changing the starting  $J$  and  $H$  magnitudes. All other parameters were computed as described in §5.2.1.

Figure 11 compares the observed age distribution derived from the HR diagram with the results from the Monte Carlo simulation. As expected, the peak of the simulated distribution decreases and more power is seen in the wings as a larger age spread is injected into the population. We have run a  $\chi^2$  test between central peaks of the data and the simulated model distributions between  $\log(age)=6$  and  $\log(age)=7.4$ . We find that the computed  $\chi^2$  probability remains high, between 50% and 60%, for simulations with an age spread of  $\leq \pm 2$  Myr, and then falls off rapidly with probabilities of  $< 5\%$  beyond  $\pm 3$  Myr. Thus, we conclude that the observed low mass population of USco formed in  $< 6$  Myr, and most likely  $< 4$  Myr; this finding is much less than the  $> 10$  Myr age spread implied by literal interpretation of the HR diagram.

### 5.3. The Low-Mass IMF

In this section we use model tracks to derive the first spectroscopic mass function for stars and brown dwarfs in USco less massive than  $\sim 0.1 M_\odot$ . The study by Preibisch et al. (2002) derived an IMF for the *stellar* population in the association by combining the 166 spectroscopically confirmed low mass members ( $M \sim 0.8-0.1 M_\odot$ ) discovered via their 2dF survey with the 120 known Hipparcos members (constituting a complete sample of members more massive than  $\sim 1 M_\odot$ ) and 84 X-ray selected members ( $M \sim 0.8-2 M_\odot$ ; Preibisch & Zinnecker 1999). The resultant mass function yielded a 3-segment power law function that was consistent with recent field star and other cluster IMF determinations above  $\sim 2 M_\odot$ , but with a  $2\sigma$  excess of stars above numbers seen in the field at lower masses.

The only previous survey that has attempted to derive an IMF for USco’s substellar members is the photometric study by Lodieu et al. (2007). These authors observed  $\sim 6.5$  deg<sup>2</sup> of USco at *ZYJHK*-bands as part of

the UKIRT Infrared Deep Sky Survey (UKIDSS) Galactic Cluster Survey. From these data, the authors used the  $J$ -band luminosity function to derive a *photometric* IMF in USco from 0.3–0.007  $M_{\odot}$ . They derived a mass function that was significantly flatter ( $dN/dM \propto M^{-0.3 \pm 0.1}$ ) than the IMF derived by Preibisch et al. (2002) for similar mass ranges ( $dN/dM \propto M^{-0.9 \pm 0.2}$  for  $0.1 \leq M/M_{\odot} < 0.6$ ). However, as noted in Slesnick et al. (2004), photometrically derived IMFs suffer from degeneracies between mass, age, distance, extinction, and photometric excess present in the CMDs from which they are derived, and they cannot directly (only statistically) correct for field star contamination.

As was discussed in §5.2, deriving quantities from spectroscopic data placed onto an HR diagram has its own set of uncertainties. We have already shown that known uncertainties in observable magnitudes and spectral types can produce an apparent age spread of  $>10$  Myr, and therefore must also determine if uncertainties in the data can produce a false spread in the observed mass distribution. To address this issue, we derived a theoretical IMF for a coeval population of stars at 5 Myr. We assumed a spectral type distribution consistent with that for our observed population, and assigned each star the mass that it would have at that spectral type if it were 5 Myr-old. Examination of the difference between the two mass distributions using a KS test reveals that the mass distributions derived from the data and the theoretical 5 Myr-old population are statistically consistent with each other (probability=12%). Because the mass tracks are close to vertical for low mass stars (see Figure 8), the dominant source of uncertainty in derived masses will come from uncertainties in temperature, arising from uncertainties in spectral type ( $\pm 0.5$  subtypes). Presuming we are equally likely to misclassify a star 0.5 subtypes too early as we are to misclassify it 0.5 subtypes too late, the mass distribution will not change significantly. Thus, we conclude that the mass distribution derived from the HR diagram is robust to observable uncertainties. We note, however, that the mass distribution is strongly affected by systematics in the theoretical models, and results will vary dependent upon which set of mass tracks are used.

In Figure 12, we show the IMF derived using the DM97 models for our spectroscopic survey of low mass stars and brown dwarfs, covering the mass range  $M \sim 0.2$ – $0.02 M_{\odot}$ . Because we have observed spectroscopically only  $\sim 15\%$  of the photometric PMS star candidates, before constructing a mass function, it is necessary to determine that the spectroscopic sample presented here is representative of the USco low mass population as a whole. We use a method similar to that employed by Slesnick et al. (2004) and determine the relative completeness of our sample by computing the number of stars observed spectroscopically compared to the number of photometric candidates present in uniformly-spaced bins perpendicular to the line of selection at the 1% data contour (see Figure 1). As can be seen, the number of observed stars falls off considerably for stars with magnitudes  $r \gtrsim 19.5$  which could be observed only under the best seeing conditions. The spectroscopic survey completeness peaks at  $\sim 20\%$ . We correct the IMF to uniform completeness at this level by determining the mass distribution of stars within each magnitude bin. We then add stars to the relevant mass bins based on the fractional completeness

of the magnitude bins they came from, relative to the maximum 20% completeness level.

In order to extend our sample to higher masses, we combined masses derived for our sample with those for stars from the survey by Preibisch et al. (2002). We chose to use the Preibisch et al. (2002) sample because (1) it constitutes the largest sample of spectroscopically confirmed low mass stellar members, and (2) candidates were selected from an  $I, R - I$  CMD in a manner similar to the methods employed to select our sample thus providing a complementary dataset. We specifically chose not to include the higher mass X-ray selected sources (Preibisch & Zinnecker 1999) due to the large difference in selection techniques. To provide the most analogous samples possible, we re-derived masses for the 160 stars in the Preibisch et al. (2002) survey with M spectral types by first converting published spectral types and 2MASS magnitudes to temperature and luminosity using the techniques described in §5.1, and then using the DM97 tracks and the same interpolation program used to generate masses for the sample of stars presented here. In combining samples from multiple sources, one must be careful to account for relative completeness. Preibisch et al. (2002) estimate spectroscopic completeness levels of 87% for stars with  $0.2 < M/M_{\odot} < 0.8$  and 67% for stars with mass  $< 0.2 M_{\odot}$ , whereas, our corrected survey is only 20% complete across all sampled mass bins. The number of stars in the Preibisch et al. (2002) survey were thus multiplied by either (20% complete/87% complete) for stars with  $0.2 < M/M_{\odot} < 0.8$ , or (20% complete/67% complete) for stars with  $M < 0.2 M_{\odot}$ . The two surveys also cover very different areas. Preibisch et al. (2002) looked at  $9 \text{ deg}^2$  whereas the Quest-2 survey looked at  $\sim 150 \text{ deg}^2$ . However, as discussed in Paper I, SCH06, and Slesnick (2007), the Quest-2 survey coverage within this area is not complete due to several failed CCDs, gaps between the CCDs, and incomplete  $r-i$  color coverage. To account for differences in area, we scaled the IMF derived from the Preibisch et al. (2002) data to match, on average, the level of the IMF derived from stars in our survey in the  $-0.6 > \log(M/M_{\odot}) > -1.0$  mass bins. Due to the nature of magnitude limited surveys, the lowest mass bin (or bins, depending on bin-width) of any IMF is usually incomplete relative to the rest of the derived distribution; thus, for the IMF in the combined samples, we use the values derived from the Quest-2 data to populate the  $-1.0 > \log(M/M_{\odot}) > -1.4$  bins of the IMF.

Figure 14 shows IMFs for the low mass stellar and substellar population of the USco association. In total, the combined IMF contains  $\sim 377$  stars with masses as high as  $\sim 0.6 M_{\odot}$  and as low as  $< 0.02 M_{\odot}$ . The derived mass function rises with a slope of  $dN/dM \propto M^{-1.13}$ , peaks at  $\sim 0.13 M_{\odot}$ , remains high with a secondary peak at  $M \sim 0.05 M_{\odot}$ , and then gradually falls off through the substellar regime. Thus, we find the spectroscopic IMF for USco's low mass population to be very different from the photometric IMF derived by Lodieu et al. (2007) which had a flatter slope  $dN/dM \propto M^{-0.3}$  from  $0.3 < M/M_{\odot} < 0.01$ , and peaked at  $M \sim 0.01 M_{\odot}$ . The total mass inferred from the spectroscopic IMF over the mass range  $0.6$ – $0.02 M_{\odot}$  is  $\sim 48 M_{\odot}$ . If we correct this number to account for the fact that the IMF shown here is only 20% complete over  $\sim 40\%$  of the entire spatial extent of the Hipparcos stars, the total mass inferred for

association members less massive than  $\sim 0.6 M_{\odot}$  is  $\sim 600 M_{\odot}$ .

#### 5.4. Comparisons of the Low Mass IMF between Star-Forming Regions

Diagnostic studies of stellar populations in different locations and at varying stages of evolution are needed to explore the possibility of a universal mass function for low mass objects. While one might expect that the IMF should vary with star formation environment, we do not yet have enough evidence to determine if such a variation exists. Aside from the work presented here, numerous studies have been carried out to characterize the low mass stellar and substellar mass functions of other young clusters and associations in a variety of environments. Because of the intrinsic faintness of low mass objects, most surveys are photometric. Authors then use a combination of theoretical models and statistical analysis to transform a group's color-magnitude diagram or luminosity function into a photometric IMF which may not accurately represent the underlying population. Spectroscopic surveys provide a more accurate assessment of the stellar membership and thus, of the underlying cluster population.

The substellar populations of several other young star-forming regions have been studied spectroscopically using techniques similar to those presented here, and we discuss results for USco in comparison to three other regions. Luhman et al. (2003b) studied the rich cluster IC 348 in Perseus. There have been several studies of the Taurus region, namely those by Luhman (2000), Briceño et al. (2002), Luhman et al. (2003a), and Luhman (2004), which together constitute a complete sample within a selected region. Slesnick et al. (2004) used near-infrared imaging and spectroscopic observations to constrain the low mass IMF in the  $\sim 1$  Myr-old Orion Nebula Cluster (ONC). The data for IC 348 (Luhman et al. 2003b) and Taurus (Luhman 2000, Briceño et al. 2002, Luhman et al. 2003a, and Luhman 2004) are published as complete across all mass ranges within the areas surveyed. Slesnick et al. (2004) employed similar techniques to those used here to correct the derived IMF to a uniform 40% completeness across all magnitude ranges. IC 348, Taurus, and the ONC are all young ( $age \lesssim 3$  Myr), and, similar to USco, have not yet had time to lose members through dynamical ejection. Therefore, if the low mass IMF is universal, similar mass distributions should be observed in all four regions.

Our goal in this section is to assess the physical differences between stars formed in different star-forming environments. As described in §5.1, effective temperatures shown in Figure 8 are derived directly from observed spectral types using a theoretical or (in our case) empirical temperature scale. Observational evidence suggests that late-type young stars will have a similar mass across a large range of ages. For example, similar masses of  $M \sim 0.03\text{--}0.09 M_{\odot}$  have been measured for M6–M7 binary or triple components in both the ONC ( $\sim 1$  Myr; Stassun et al. (2006)) and AB Dor ( $\sim 75$  Myr; Close et al. (2007)). Thus, spectral type distributions should provide a reasonable approximation to mass distributions for young low mass stars. We therefore begin this exercise by first comparing spectral type distributions found in different star forming regions, and

thereby avoid introducing uncertainties that inherently arise when deriving stellar masses.

Spectral type distributions are shown in Figure 15. All four distributions are complete in a relative sense across spectral type bins for M-type stars. Distributions for members of the ONC and members of USco discovered with Quest-2 were corrected to a uniform completeness level in a manner similar to that described in §5.3. We have included in the IC 348 and Taurus spectral-type distributions all M-type stars present in the IMF of the respective discovery paper. As can be seen, the distribution for USco is visually dissimilar to the other regions, even considering the small sample sizes and large error bars. This difference could be due to real variation in the IMF, but could also be influenced by the difference in age of a few million years ( $\sim 5$  Myr vs.  $\lesssim 3$  Myr) between USco and the other regions. We performed  $\chi^2$  tests between all four distributions to determine the probabilities that the distributions could have been drawn from the same population. The tests yielded a very small probability ( $\sim 10^{-22}$ ) that the USco and ONC distributions could be drawn from the same population, and marginally-small probabilities at the 5–10% levels of USco arising from the same population as either Taurus or IC 348. However, we caution against taking results from the  $\chi^2$  test at face value. The histograms for USco and the ONC have been scaled to account for incompleteness in magnitude and spatial area during the observations, and correctly and rigorously accounting for these scaling factors in the  $\chi^2$  test is a non-trivial and not straight-forward exercise. The Taurus and IC348 populations, however, have not been scaled, and have an almost 100% chance of being drawn from the same population. While this result argues for a common spectral-type distribution between these two regions among the lowest mass stars and brown dwarfs, substantial variation was found by Luhman et al. (2003b) for hotter, K-type stars.

We now compare directly mass distributions for the four selected star forming regions. As discussed above and in §5.1, the mass of a star is inferred from placement on an HR diagram using a set of theoretical mass tracks, and the exact method by which the mass is derived can vary significantly from study to study. Thus, direct comparison of the published mass data itself requires great caution given that different mass tracks, temperature scales, and interpolation methods were used for different studies. Quantitative assessment of the differences between theoretical PMS star models is beyond the scope of this work, as is analysis of differences between the numerous temperature scales employed by various authors who study young low mass stars. We have used published spectral types and 2MASS  $J, H, K_S$  magnitudes to derive effective temperatures, luminosities, and hence masses in a manner consistent with that used in our work in the ONC and USco. We reiterate that masses for all stars presented in this section were derived in a consistent manner; however, variations in the theoretical or empirical scales/tracks used could shift interpretation of the data.

IMFs derived from the DM97 tracks are shown in Figures 16. We find that the ONC, IC 348, and Taurus IMFs exhibit a fall-off of stars beyond  $\sim 0.1 M_{\odot}$ . The mass distribution for USco, however, does not begin to turnover until  $\sim 0.05 M_{\odot}$ . Thus, similar to the spectral

type distribution, the IMF derived for USco shows an over-abundance of late-type, low mass stars, and suggests that the difference seen in USco's spectral type distribution did arise from a difference in its IMF, rather than from slight differences in age between USco and the other regions. Our work extends the claim by Preibisch et al. (2002) that USco may contain anomalously high numbers (compared to the field) of low mass stars to lower masses, and is suggestive that USco also contains relatively higher numbers of very low mass stars and brown dwarfs compared to other nearby star-forming regions.

USco differs from IC 348, Taurus and the ONC in that it contains  $\sim 50$  very massive, O- and B-type stars, almost three times the number found in the ONC (none are found in either Taurus or IC 348). Thus, the conclusion that USco may contain relatively more very low mass stars than other young regions may be related to its large number of high mass stars. For example, Adams et al. (2006) have shown through numerical simulation that disks around lower mass stars are more susceptible to destruction (further out than  $\sim 10$  AU) from dynamical interactions with surrounding stars of higher mass. It is possible that in a similar manner, low mass cores moving through a giant molecular cloud are more susceptible to stripping of their accretion envelope in the presence of higher mass cores. Our results suggest that, within a star forming region, either the presence of large numbers of very massive stars, or the environmental conditions that lead to numerous massive star formation, may play a large role in determining the low mass IMF. We note that this conclusion has been drawn from results for only four different environments. Many more regions must be studied before a definitive explanation of the low mass IMF can be derived.

## 6. SUMMARY

We have completed a large-area  $g, r, i$  photometric survey of  $\sim 150$  deg<sup>2</sup> in and near the Upper Scorpius region

of recent star formation. From these data, combined with 2MASS near-infrared magnitudes, we selected candidate new PMS association members. We present here spectral observations for a total of 243 candidates observed at either Palomar or CTIO, from which we determined 145 ( $\sim 60\%$ ) to be bona fide new Upper Scorpius members. We measured H $\alpha$  emission for all new members and determine 15 of the 145 low mass stars and brown dwarfs in the 5 Myr USco association are still accreting. Based on comparison of the spatial distributions of low and high mass association members, we find no evidence for spatial segregation in USco within the northern portion of the association.

We used photometry and spectral types to derive effective temperatures and luminosities, and placed newly identified association members onto an HR diagram. These data were combined with pre-main sequence evolutionary models to derive a mass and age for each star. Using Monte Carlo simulations we showed that, taking into account known observational errors, the observed age dispersion for the low mass population in USco is consistent with all stars forming in a single burst  $\sim 5$  Myr ago, and place an upper limit of  $\pm 3$  Myr (i.e., 60%) on the age spread if the star formation rate has been constant in time. We also derived the first spectroscopic mass function for USco that extends into the substellar regime and compared these results to those for three other young clusters and associations.

## 7. APPENDIX A

Magnitudes for the Quest-2 photometric candidates spectroscopically determined to be field stars are listed in Table 3.

*Facilities:* PO:1.2m (Quest-2), Hale (Double Spectrograph), Blanco (Hydra)

## REFERENCES

- Adams, F. C., Proszkow, E. M., Fatuzzo, M., & Myers, P. C. 2006, *ApJ*, 641, 504
- Ardila, D., Martín, E., & Basri, G. 2000, *AJ*, 120, 479
- Baltay, C., Rabinowitz, D., Andrews, P., Bauer, A., Ellman, N., Emmet, W., Hudson, R., Hurteau, T., Jerke, J., Lauer, R., Silge, J., Szymkowiak, A., Adams, B., Gebhard, M., Musser, J., Doyle, M., Petrie, H., Smith, R., Thicksten, R., & Geary, J. 2007, *PASP*, 119, 1278
- Baraffe, I., Chabrier, G., Allard, F., & Hauschildt, P. H. 1998, *A&A*, 337, 403
- Barrado y Navascués, D. & Martín, E. L. 2003, *AJ*, 126, 2997
- Barsony, M., Kenyon, S. J., Lada, E. A., & Teuben, P. J. 1997, *ApJS*, 112, 109
- Bessell, M. S. & Brett, J. M. 1988, *PASP*, 100, 1134
- Briceño, C., Luhman, K. L., Hartmann, L., Stauffer, J. R., & Kirkpatrick, J. D. 2002, *ApJ*, 580, 317
- Carpenter, J. M. 2000, *AJ*, 120, 3139
- Close, L. M., Thatte, N., Nielsen, E. L., Abuter, R., Clarke, F., & Tecza, M. 2007, *ApJ*, 665, 736
- D'Antona, F. & Mazzitelli, I. 1997, *Memorie della Societa Astronomica Italiana*, 68, 807
- de Bruijne, J. H. J. 1999, *MNRAS*, 310, 585
- de Zeeuw, P. T., Hoogerwerf, R., de Bruijne, J. H. J., Brown, A. G. A., & Blaauw, A. 1999, *AJ*, 117, 354
- Gomez, M., Hartmann, L., Kenyon, S. J., & Hewett, R. 1993, *AJ*, 105, 1927
- Guiou, S., Dougados, C., Monin, J.-L., Magnier, E., & Martín, E. L. 2006, *A&A*, 446, 485
- Haisch, Jr., K. E., Lada, E. A., & Lada, C. J. 2001, *ApJ*, 553, L153
- Hillenbrand, L. A. 2005, *astro-ph*, 0511083
- Hillenbrand, L. A., Bauermeister, A., & White, R. J. 2008, in *Astronomical Society of the Pacific Conference Series*, Vol. 384, 14th Cambridge Workshop on Cool Stars, Stellar Systems, and the Sun, ed. S. P. P. S. D. E. M. B. J. Messina, 200
- Hillenbrand, L. A. & White, R. J. 2004, *ApJ*, 604, 741
- Kraus, A. L., Ireland, M. J., Martinache, F., & Lloyd, J. P. 2008, *ApJ*, 679, 762
- Kraus, A. L., White, R. J., & Hillenbrand, L. A. 2005, *ApJ*, 633, 452
- Lada, C. J. & Lada, E. A. 2003, *ARA&A*, 41, 57
- Lada, E. A. & Lada, C. J. 1995, *AJ*, 109, 1682
- Leggett, S. K., Allard, F., Berriman, G., Dahn, C. C., & Hauschildt, P. H. 1996, *ApJS*, 104, 117
- Leggett, S. K., Golimowski, D. A., Fan, X., Geballe, T. R., Knapp, G. R., Brinkmann, J., Csabai, I., Gunn, J. E., Hawley, S. L., Henry, T. J., Hindsley, R., Ivezić, Ž., Lupton, R. H., Pier, J. R., Schneider, D. P., Smith, J. A., Strauss, M. A., Uomoto, A., & York, D. G. 2002, *ApJ*, 564, 452
- Lodieu, N., Hambly, N. C., Jameson, R. F., & Hodgkin, S. T. 2008, *MNRAS*, 383, 1385
- Lodieu, N., Hambly, N. C., Jameson, R. F., Hodgkin, S. T., Carraro, G., & Kendall, T. R. 2007, *MNRAS*, 374, 372
- Loinard, L., Torres, R. M., Mioduszewski, A. J., & Rodríguez, L. F. 2008, *ApJ*, 675, L29
- Luhman, K. L. 2000, *ApJ*, 544, 1044
- . 2004, *ApJ*, 617, 1216
- Luhman, K. L., Briceño, C., Stauffer, J. R., Hartmann, L., Barrado y Navascués, D., & Caldwell, N. 2003a, *ApJ*, 590, 348

- Luhman, K. L., Stauffer, J. R., Muench, A. A., Rieke, G. H., Lada, E. A., Bouvier, J., & Lada, C. J. 2003b, *ApJ*, 593, 1093
- Mamajek, E. E., Meyer, M. R., Hinz, P. M., Hoffmann, W. F., Cohen, M., & Hora, J. L. 2004, *ApJ*, 612, 496
- Martín, E. L., Delfosse, X., & Guieu, S. 2004, *AJ*, 127, 449
- Massey, P., Strobel, K., Barnes, J. V., & Anderson, E. 1988, *ApJ*, 328, 315
- Preibisch, T., Brown, A. G. A., Bridges, T., Guenther, E., & Zinnecker, H. 2002, *AJ*, 124, 404
- Preibisch, T., Guenther, E., & Zinnecker, H. 2001, *AJ*, 121, 1040
- Preibisch, T., Guenther, E., Zinnecker, H., Sterzik, M., Frink, S., & Roeser, S. 1998, *A&A*, 333, 619
- Preibisch, T. & Zinnecker, H. 1999, *AJ*, 117, 2381
- Preibisch, T. & Zinnecker, H. 2007, in *IAU Symposium*, Vol. 237, IAU Symposium, ed. B. G. Elmegreen & J. Palous, 270–277
- Rabinowitz, D., Baltay, C., Emmet, W., Hurteau, T., Snyder, J., Andrews, P., Ellman, N., Morgan, N., Bauer, A., Musser, J., Gebhard, M., Adams, G., Djorgovski, G., Mahabal, A., Graham, M., Bogosavljevic, M., Williams, R., Brucato, R., & Thicksten, R. 2003, in *Bulletin of the American Astronomical Society*, 1262
- Salpeter, E. E. 1955, *ApJ*, 121, 161
- Shu, F. H., Adams, F. C., & Lizano, S. 1987, *ARA&A*, 25, 23
- Skrutskie, M. F., Cutri, R. M., Stiening, R., Weinberg, M. D., Schneider, S., Carpenter, J. M., Beichman, C., Capps, R., Chester, T., Elias, J., Huchra, J., Liebert, J., Lonsdale, C., Monet, D. G., Price, S., Seitzer, P., Jarrett, T., Kirkpatrick, J. D., Gizis, J. E., Howard, E., Evans, T., Fowler, J., Fullmer, L., Hurt, R., Light, R., Kopan, E. L., Marsh, K. A., McCallon, H. L., Tam, R., Van Dyk, S., & Wheelock, S. 2006, *AJ*, 131, 1163
- Slesnick, C. L. 2007, PhD thesis, California Institute of Technology
- Slesnick, C. L., Carpenter, J. M., & Hillenbrand, L. A. 2006a, *AJ*, 131, 3016 (Paper I)
- Slesnick, C. L., Carpenter, J. M., Hillenbrand, L. A., & Mamajek, E. E. 2006b, *AJ*, 132, 2665 (SCH06)
- Slesnick, C. L., Hillenbrand, L. A., & Carpenter, J. M. 2004, *ApJ*, 610, 1045
- Stassun, K. G., Mathieu, R. D., & Valenti, J. A. 2006, *Nature*, 440, 311
- Wilking, B. A., Schwartz, R. D., & Blackwell, J. H. 1987, *AJ*, 94, 106

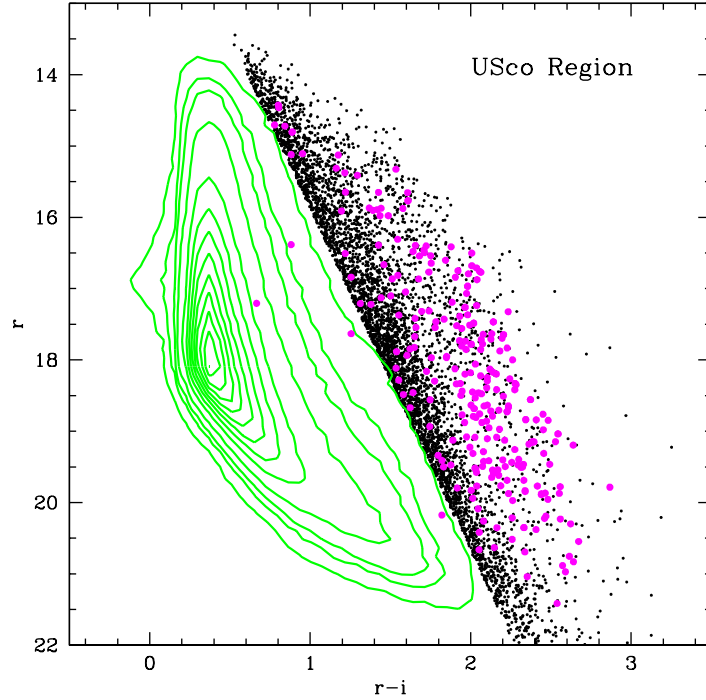


FIG. 1.— Optical color-magnitude diagram of all Quest-2 sources in the final USco catalog with  $riJHK_S$  detections. Contours represent the density of sources in the diagram, with contour levels at 1%, 2%, 5%, and 10–90% of the peak value. Objects red-ward of a linear approximation of the 1% contour are shown as discrete points. Objects for which we have spectral data are shown as large symbols. Photometry for four of the targets has changed significantly since the first spectroscopic observations were taken (see SCH06) such that they would no longer be considered candidates.

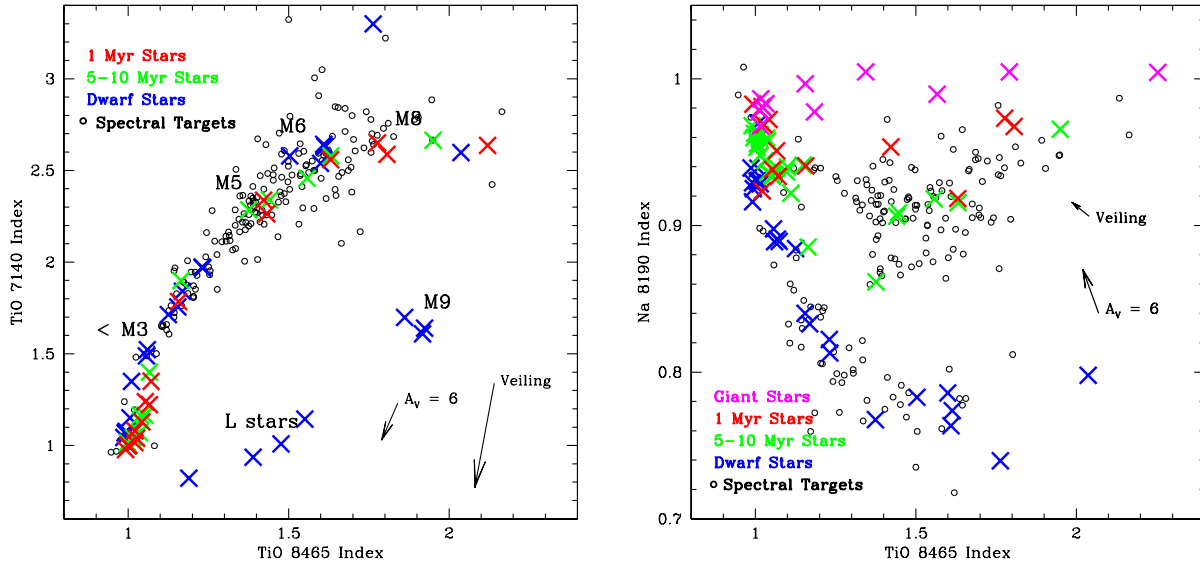


FIG. 2.— Left panel shows temperature-sensitive TiO-7140 vs. TiO-8465 indices; right panel shows TiO-8465 index vs. gravity sensitive Na-8190 index. In both panels, blue X's represent measured indices for a sample of old stars comprised of field dwarfs and members of the Hyades ( $\sim 650$  Myr), Pleiades ( $\sim 115$  Myr) and AB Dor ( $\sim 75$ – $150$  Myr) associations. Green X's show measured indices for intermediate-age spectral standards from Beta Pic ( $\sim 11$  Myr), TW Hya ( $\sim 8$  Myr), and Upper Sco ( $\sim 5$  Myr). Red X's show measured indices for young Taurus members ( $\sim 1$ – $2$  Myr). Magenta X's in the right panel represent measured indices for giant standard stars. In both panels, black circles are measured indices for USco PMS candidates observed at Palomar. The effects of extinction and veiling are shown as vectors (see Paper I and SCH06).

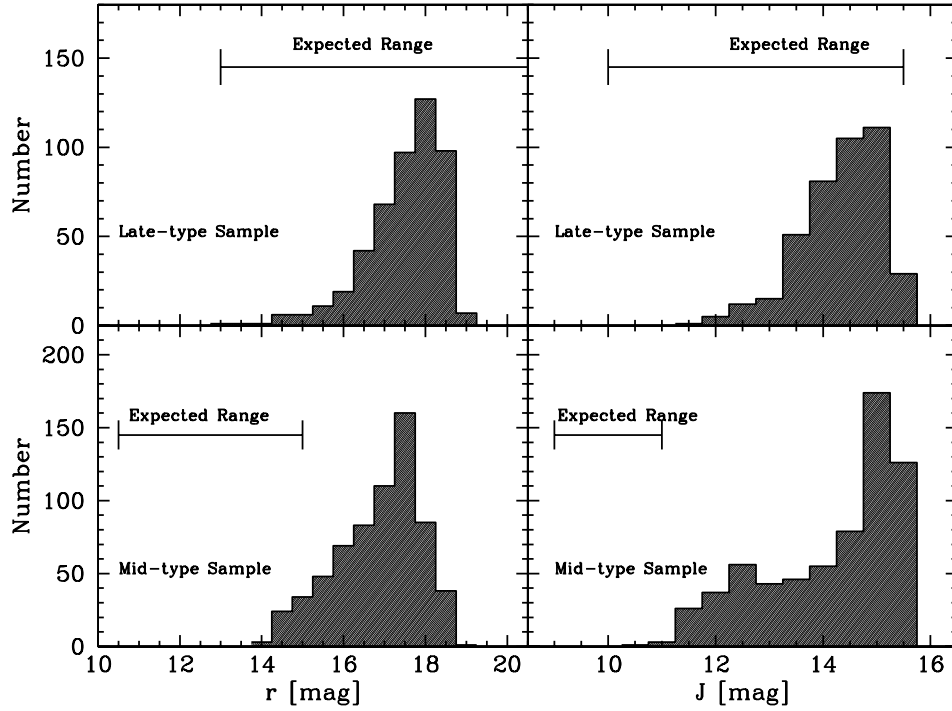


FIG. 3.— Histograms of  $r$ - and  $J$ -band magnitudes for targets of the Hydra spectral observations. The top histograms show data for stars classified as spectral type late-K to M; the bottom histograms show data classified as spectral type late F to early-K. Shown in both panels is the expected range of magnitudes for 5 Myr-old stars of those spectral types at the distance of USco.

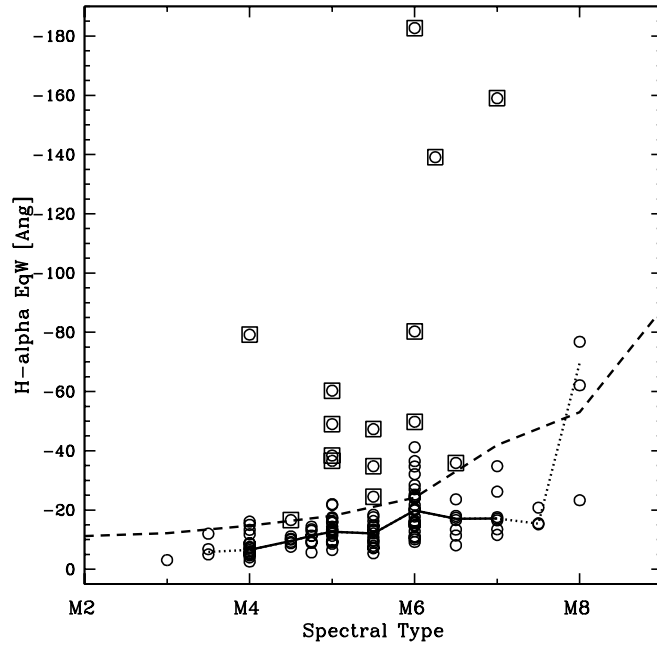


FIG. 4.— Measured  $H\alpha$  equivalent widths for all 145 low mass USco members presented here, shown as a function of spectral type. Dashed line represents the empirical accretor/nonaccretor upper limit derived by Barrado y Navascués & Martín (2003). Solid line represents the median  $W(H\alpha)$  for each spectral type. The spectral-type bins earlier than M4 and later than M7 do not have enough measurements to derive a statistically representative value for median  $H\alpha$  emission and we do not consider any star outside the M4–M7 spectral type range to be in our sample of  $H\alpha$  excess sources. Boxed objects have  $H\alpha$  emission in excess of  $3\sigma$  above the median value for their spectral type, and are considered by us to be actively accreting.

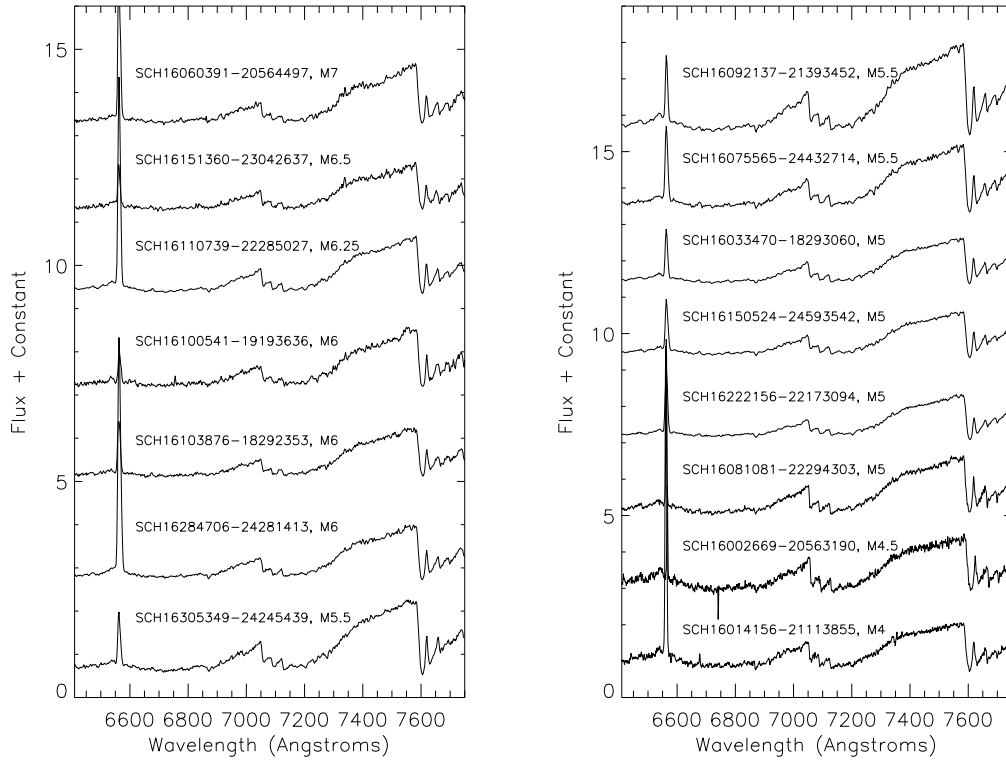


FIG. 5.— Spectra of the 15 stars determined to be accreting (as defined in §3), shown in order of decreasing spectral type.

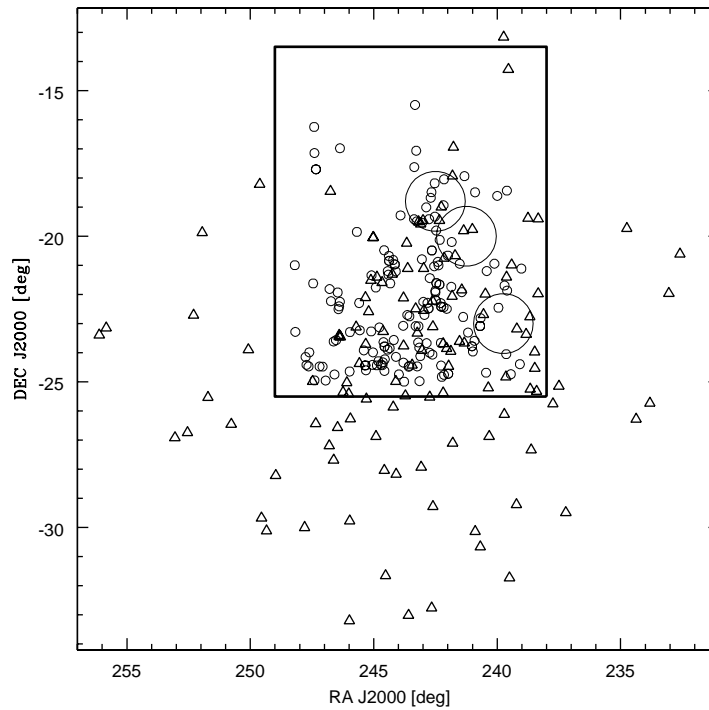


FIG. 6.— Spatial distribution of the 120 known Hipparcos members of USco (open triangle) shown with stars observed spectroscopically by us that were determined to be new members (open circles). The Quest-2 survey area is boxed in black. The approximate location and size of the 2dF fields observed by Preibisch et al. (2002) are shown as large circles.

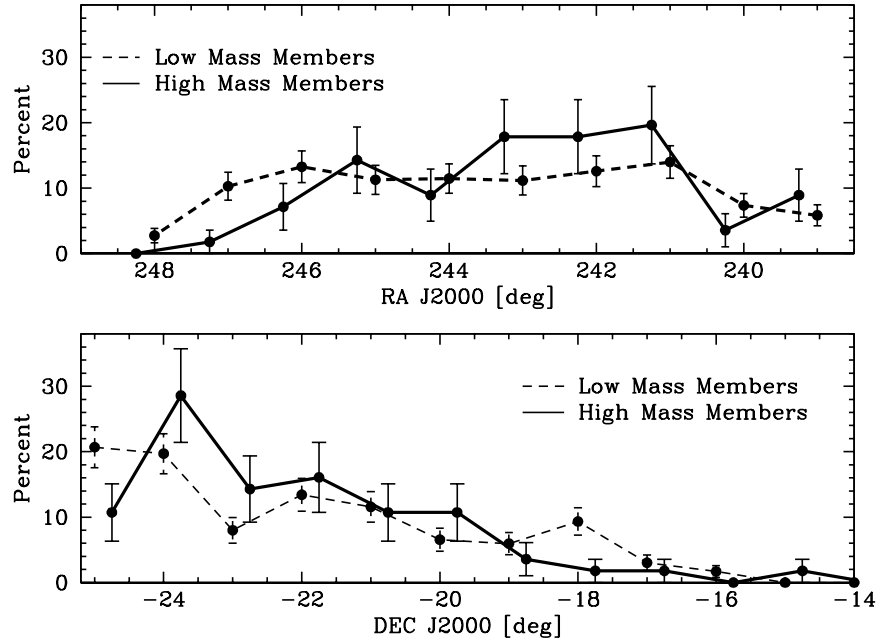


FIG. 7.— Top panel shows the percentage of the low mass stars ( $M \lesssim 0.6 M_{\odot}$ ) discovered in this work (corrected to a uniform 25% of candidates observed across all values) that lie at a given right ascension (dashed line) together with same information for the 56 high mass Hipparcos stars ( $M \gtrsim 1 M_{\odot}$ ) found in the Quest-2 survey area (solid line). Bottom panel illustrates the same information as a function of declination. In both top and bottom panels, the coordinates of the high mass star bins have been shifted by  $0.25^{\circ}$  for ease of comparison between the high and low mass samples. Errorbars assume Poisson statistics.

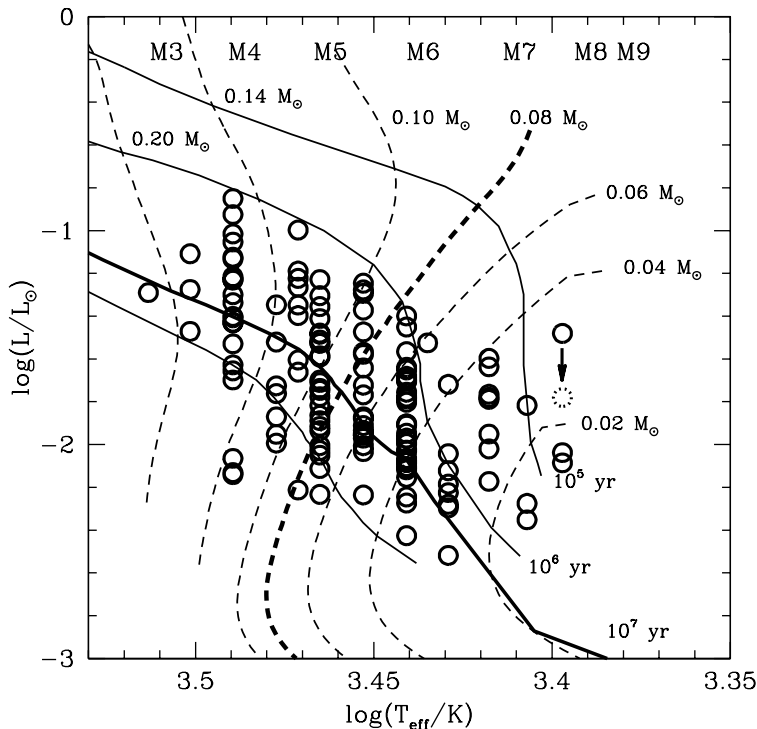


FIG. 8.— HR diagram for new PMS objects found in the USco region, shown with model tracks and isochrones of D'Antona & Mazzitelli (1997). The sample is consistent with an age of  $\sim 5$  Myr and contains masses spanning the brown dwarf to stellar regimes. The arrow plus dotted symbol indicates where the star SCH16224384-19510575 would sit in the HR diagram as a single star if it is an unresolved, equal-mass binary (see §4.2 in Paper I).

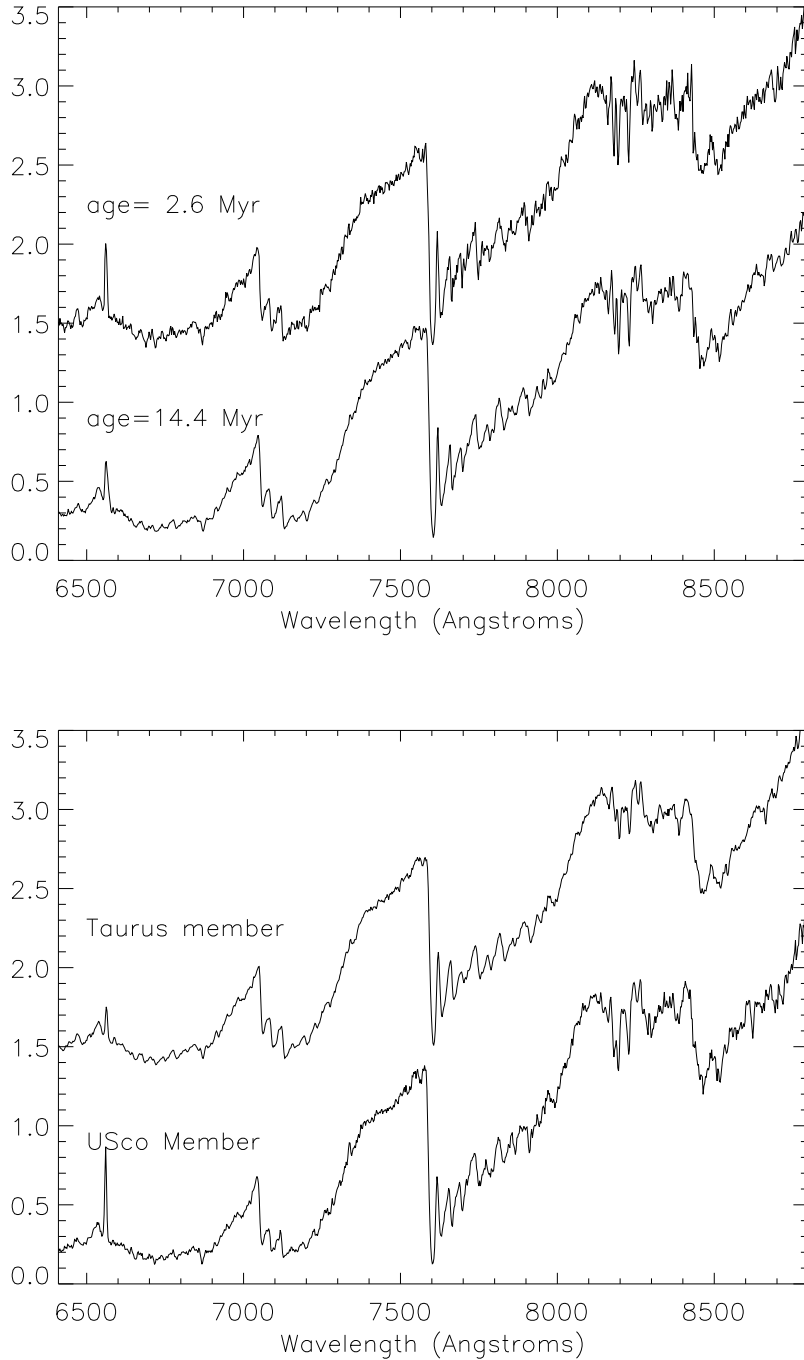


FIG. 9.— Top panel shows spectra of two stars with spectral type M5 found in the USco survey. The top spectrum is of the ‘youngest’ (based on analysis of the HR diagram) M5 star observed spectroscopically at Palomar,  $\sim 2.6$  Myr-old; the bottom spectrum is of the ‘oldest’ (based on analysis of the HR diagram) M5 star observed at Palomar,  $\sim 14.4$  Myr. However, these stars have near-identical spectra, and, based on analysis of the strength of the surface gravity sensitive Na I line (8190 Å), appear to be the same age. In the lower panel we show spectra of known members of Taurus and USco, for comparison. The two stars have measured Na-8190 indices that are different by  $\sim 9\%$ , and can be easily distinguished from each other visually.

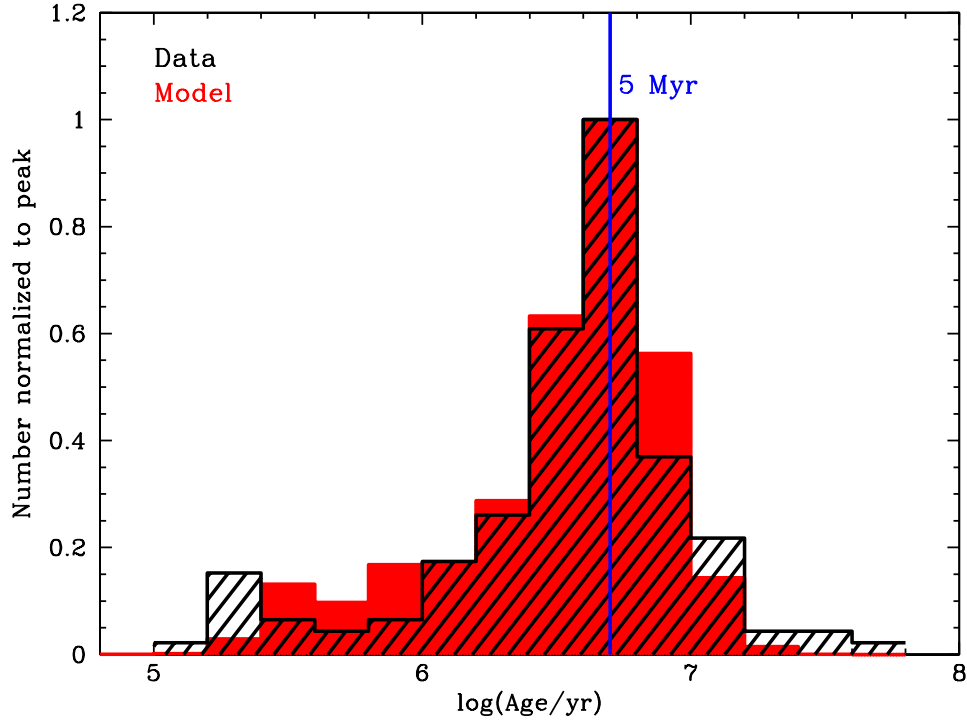


FIG. 10.— Red shaded histogram shows the age distribution derived from the Monte Carlo simulation, overplotted with a histogram of ages for the data (black hatched histogram). Both histograms have been normalized to unity at the peak for comparison, and stars having  $\log(T_{eff}) < 3.4$  (beyond which interpolation of the isochrones becomes unreliable) have been excluded from the data and the model results. The widths of the distributions are remarkably similar, given the simplistic nature of the Monte Carlo simulation.

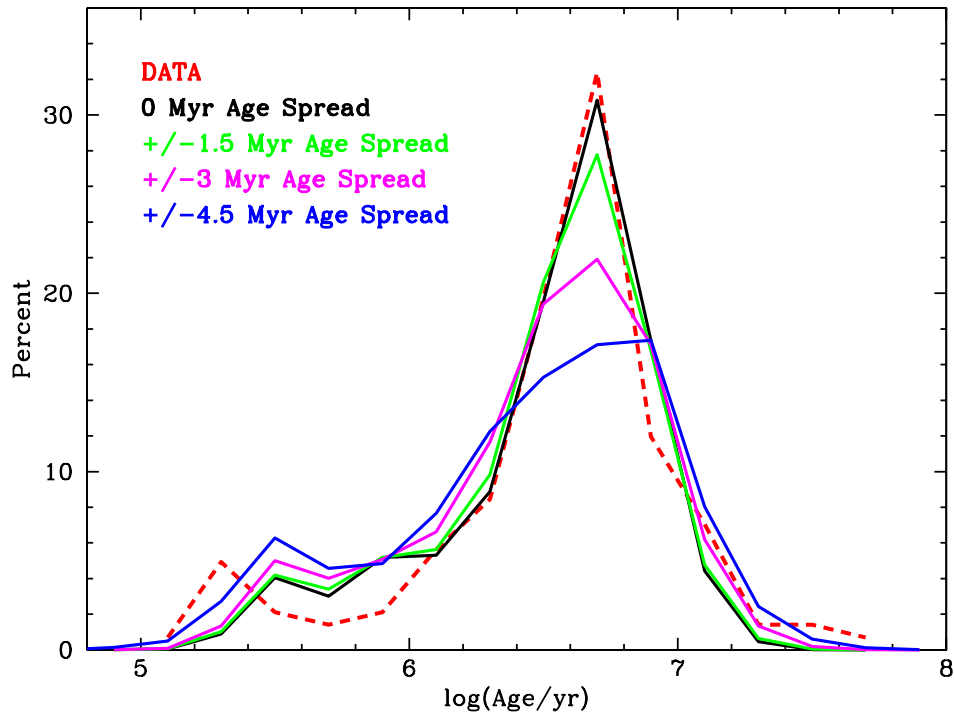


FIG. 11.— Red dashed line shows the age distribution derived from spectral data, plotted as percentage of the total stars that are at a certain age. Colored solid lines show the same information for results from the coeval model (black), together with results from model age distributions of  $5 \pm 1.5$  Myr (green),  $5 \pm 3$  Myr (magenta), and  $5 \pm 4.5$  Myr (blue). As expected, the peak of the simulated distribution decreases and more power is seen in the wings as a larger age spread is injected into the population.

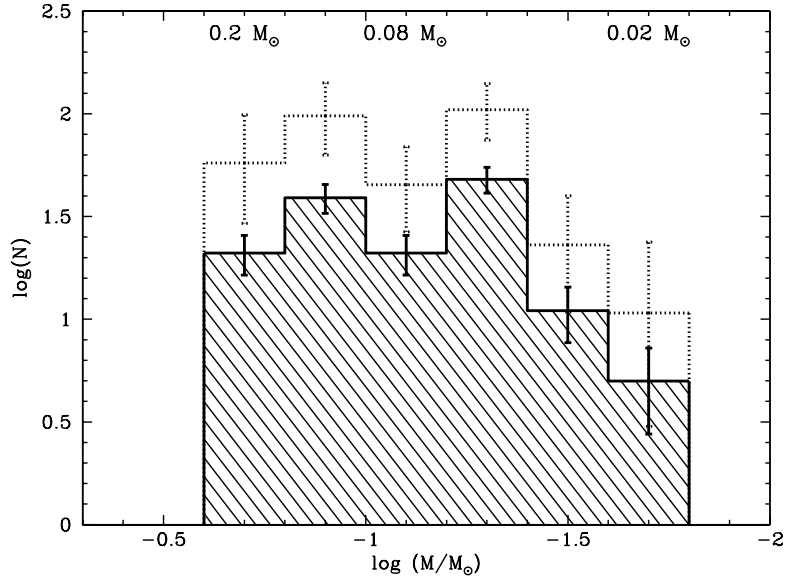


FIG. 12.— Mass function for all spectroscopically confirmed members presented in this work. Thick-lined hatched histogram indicates all stars in our spectroscopic sample; the dotted open histogram represents the same sample corrected for incomplete selection bins (§5.3).

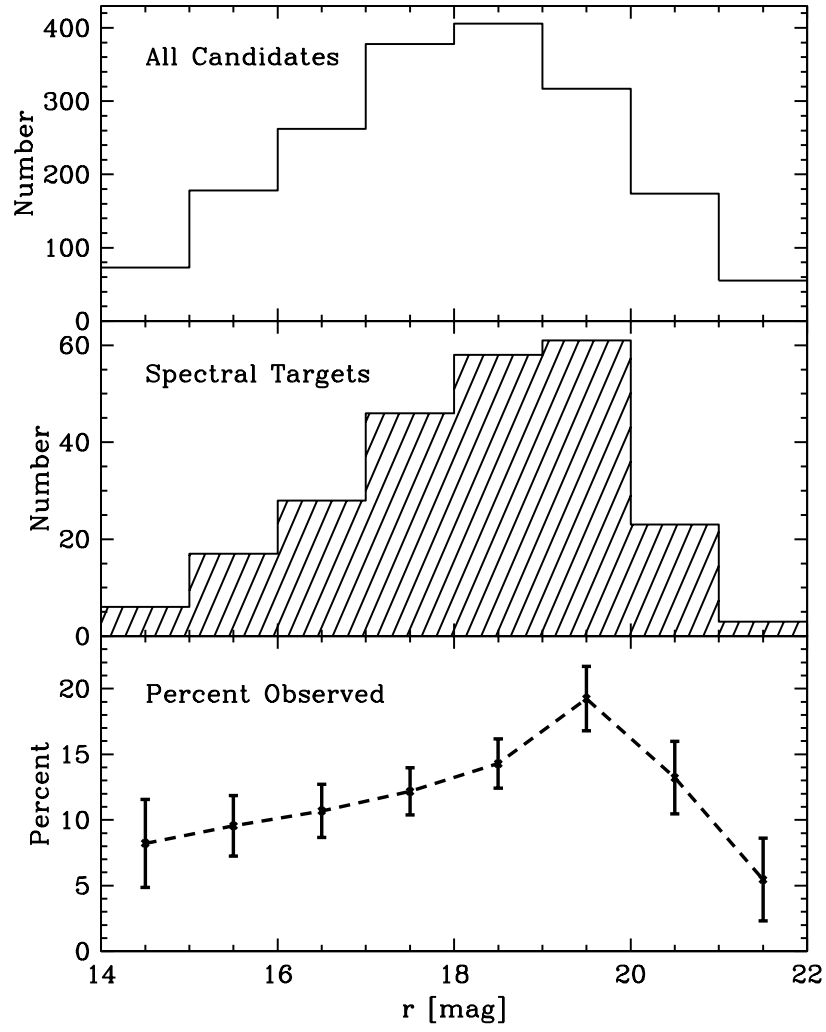


FIG. 13.— Histogram of optical CMD completeness as a function of  $r$  magnitude. Bin centers correspond to  $r$  magnitudes at the 1% contour line in Figure 1. The top panel shows data for all photometric PMS candidates selected as in §2.1, and the middle panel shows data for all targets observed spectroscopically. The bottom panel shows the percent completeness with  $\sqrt{N}$  errorbars. Completeness peaks at 20% near  $r=19.5$  mag.

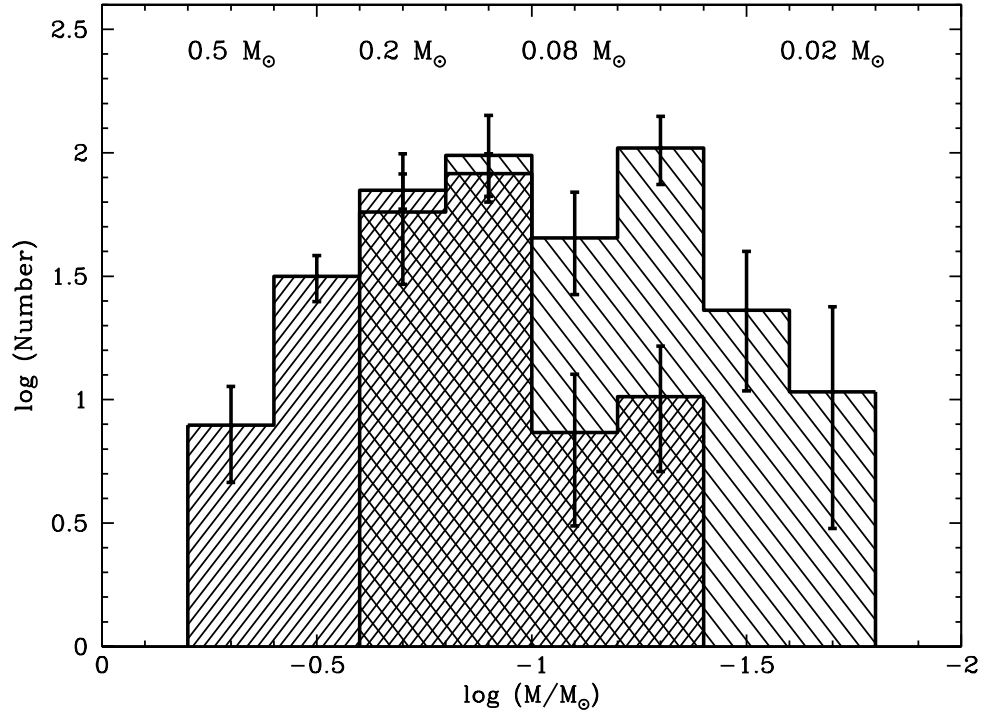


FIG. 14.— IMF for the USco association from  $\sim 0.6$ – $0.02 M_{\odot}$ . The light and dark hatched histograms depict the IMFs derived from the Quest-2 survey and the Preibisch et al. (2002) survey, respectively. Both IMFs have been scaled to a uniform 20% completeness, and data from the Preibisch et al. (2002) survey have been scaled to match the data presented here in the  $-0.6 > \log(M/M_{\odot}) > -1.0$  mass bins. All histograms are shown with  $\sqrt{N}$  errorbars.

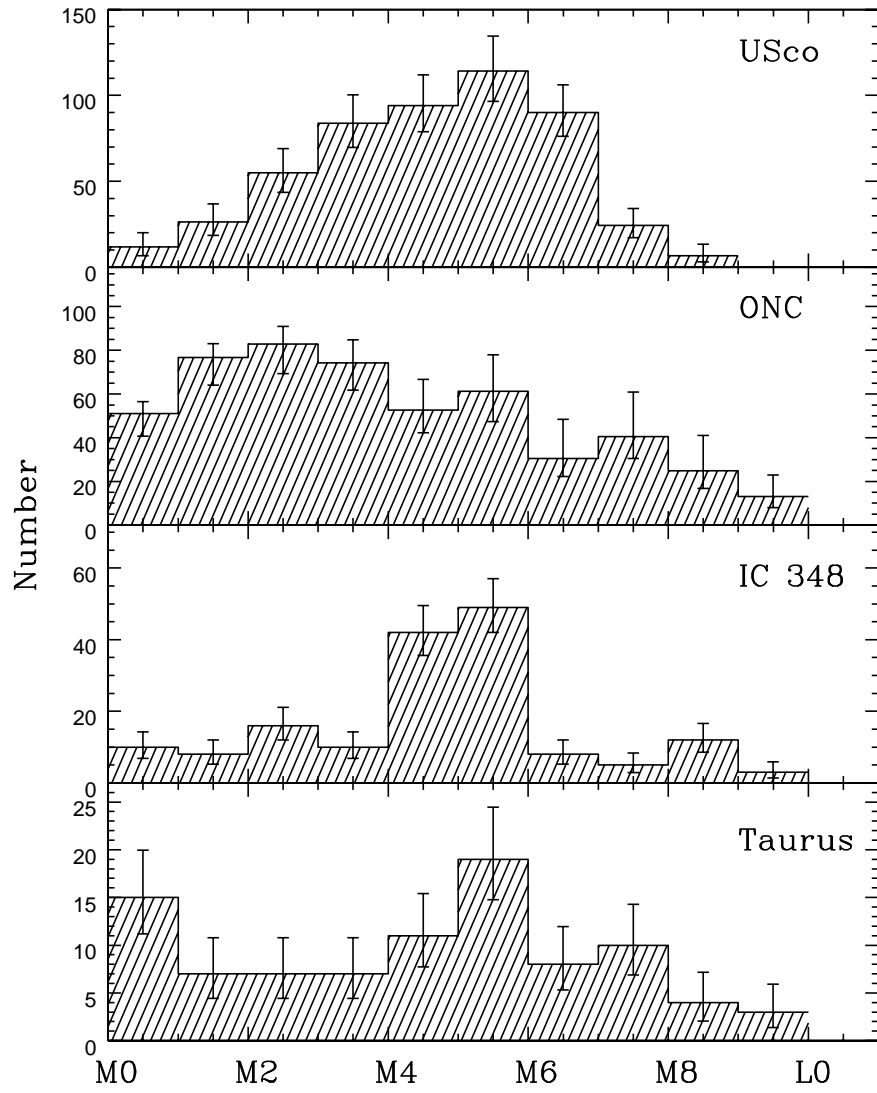


FIG. 15.— Low-mass spectral type distributions for USco, the ONC, IC 348, and Taurus. Data for the latter three regions were taken from the literature (see text).

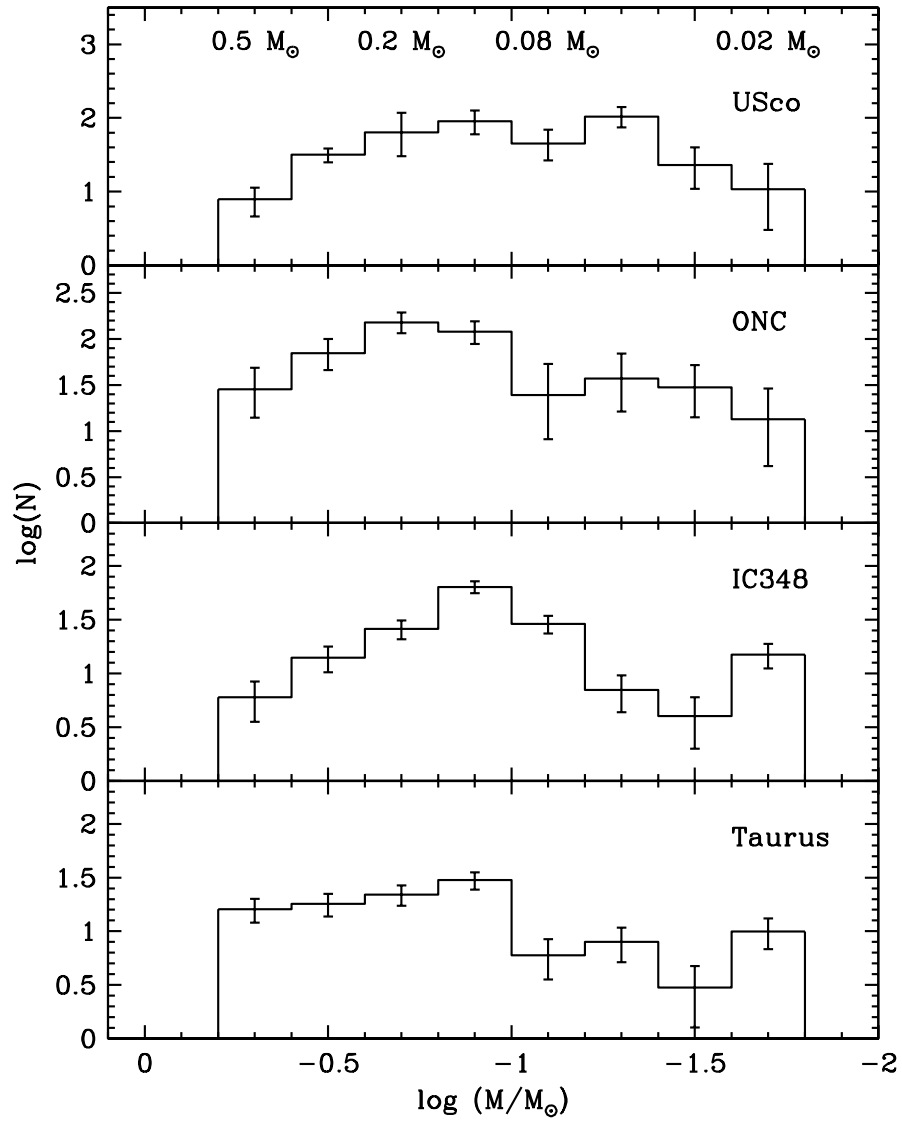


FIG. 16.— Low mass IMFs for USco, the ONC, IC 348, and Taurus generated from DM97 mass tracks. Data for the latter three regions were taken from the literature (see text).

Table 1. Measured quantities for new PMS stars in USco

ID <sup>a</sup>	g	r	i	J <sup>c</sup>	H <sup>c</sup>	K <sub>S</sub> <sup>c</sup>	TiO-7140	TiO-8465	Na-8195	SpType <sup>d</sup>	W(H $\alpha$ ) [Å]	Other identification/SpType
SCH J15560497-21064632		20.19	17.72	14.12	13.41	12.97	2.88	1.94	0.94	M7	-16.5	DENIS-P J155605.0-210646/M7 <sup>e</sup>
SCH J15561978-24232936		18.17	16.18	13.36	12.74	12.48				M4.5	-9.2	
SCH J15574757-24441236	19.02	17.37	15.81	12.98	12.36	12.05				M4	-8.8	
SCH J15582337-21515908 <sup>b,j</sup>	18.71			12.24	11.59	11.28	2.21	1.36	0.94	M4.75	-9.4	
SCH J15582566-18260865	19.59	18.17	16.03	12.92	12.20	11.79	2.55	1.57	0.92	M6	-20.2	
SCH J15583162-24025411		18.05	16.02	13.16	12.51	12.20	1.95	1.25	0.93	M4.5	-7.6	
SCH J15584812-21413426	20.23	18.53	16.50	13.48	12.87	12.51	2.39	1.42	0.87	M5.5	-10.8	
SCH J15594802-22271650 <sup>j</sup>		19.83	17.49	14.24	13.56	13.16	2.78	1.90	0.93	M7.5	-15.2	
SCH J15595868-18365205		19.15	16.76	13.43	12.76	12.40	2.48	1.53	0.91	M5.5	-14.8	
SCH J16002669-20563190	20.00	18.33	16.39	13.46	12.89	12.50				M4.5	-16.6	UScoCTIO 112/M5.5 <sup>h</sup>
SCH J16014156-21113855	19.05	17.54	15.76	12.74	12.04	11.68				M4	-79.2	
SCH J16014768-24410152 <sup>j</sup>		19.08	16.92	13.87	13.27	13.00	2.44	1.45	0.86	M5	-16.0	
SCH J16024143-22484204		18.29	16.19	13.04	12.42	11.99	2.48	1.56	0.91	M5.5	-18.4	UScoCTIO 102 <sup>h</sup>
SCH J16024576-23045102	18.91	17.46	15.32	12.46	11.84	11.50	2.33	1.38	0.87	M5	-9.6	[PBB2002] USco J160245.7-230450/M6 <sup>f</sup>
SCH J16033470-18293060	19.38	17.63	15.50	12.51	11.83	11.48	2.21	1.38	0.91	M5	-36.6	DENIS-P J160334.7-182930/M5.5 <sup>e</sup>
SCH J16034029-23352386		16.39	14.74	12.26	11.62	11.32				M4	-5.3	
SCH J16035651-23572517	19.91	18.43	16.49	13.60	13.01	12.67				M4.5	-10.3	
SCH J16040453-23463795 <sup>j</sup>	17.19	15.76	14.15	11.74	11.04	10.73	1.81	1.20	0.93	M4	-4.0	
SCH J16044303-23182620 <sup>j</sup>		19.50	17.17	13.81	13.19	12.85	2.72	1.79	0.90	M6.5	-18.0	UScoCTIO 1102 <sup>h</sup>
SCH J16051829-17562092 <sup>j</sup>	17.07	15.65	14.04	11.64	10.98	10.68	1.66	1.11	0.93	M4	-5.4	
SCH J16053077-22462016 <sup>j</sup>		19.47	17.17	13.78	13.18	12.78	2.84	1.65	0.89	M6	-17.8	
SCH J16054416-21550566		16.79	14.80	11.90	11.28	10.94	2.35	1.40	0.90	M5	-9.4	
SCH J16060391-20564497		19.43	17.18	13.52	12.90	12.47	2.77	1.89	0.95	M7	-159.0	DENIS-P J160603.9-205644/M7.5 <sup>e</sup>
SCH J16072239-20115852	19.27	17.73	15.76	12.70	12.02	11.58	2.37	1.48	0.93	M5.5	-14.2	[PBB2002] USco J160722.4-201158/M5 <sup>f</sup>
SCH J16072640-21441727		20.21	17.95	14.66	14.02	13.67	2.36	1.64	0.88	M6	-10.7	
SCH J16075565-24432714		18.68	16.66	13.83	13.13	12.71	2.13	1.46	0.90	M5.5	-47.3	
SCH J16075850-20394890 <sup>j</sup>		19.12	16.91	13.59	12.95	12.58	2.47	1.53	0.89	M6	-14.9	
SCH J16081081-22294303		17.55	15.61	12.61	11.99	11.67				M5	-49.0	
SCH J16083646-24453053	16.64	15.32	13.79	11.59	10.94	10.73				M3.5	-12.0	
SCH J16083658-18024994		18.41	16.14	12.78	12.21	11.75	2.59	1.75	0.93	M6.5	-16.6	
SCH J16084058-22255726	19.78	18.29	16.52	14.09	13.46	13.22				M4	-2.6	
SCH J16084170-18561077	19.44	17.69	15.50	12.22	11.58	11.21	2.55	1.60	0.92	M6	-10.1	[PBB2002] USco J160841.7-185610/M6 <sup>f</sup>
SCH J16085870-24493641	18.02	16.54	14.86	12.31	11.66	11.41				M4	-7.1	
SCH J16090451-22245259		19.03	16.49	13.01	12.36	11.99	2.75	1.81	0.95	M7	-17.1	
SCH J16090511-24262843		15.87	14.29	11.96	11.26	10.98				M4	-5.9	
SCH J16090771-23395430	18.57	17.06	15.09	12.08	11.44	11.13	2.30	1.39	0.92	M5	-15.7	
SCH J16090883-22174699	19.34	17.71	15.64	12.97	12.33	12.07				M5	-14.4	
SCH J16091837-20073523		17.96	16.11	13.00	12.37	12.01				M7.5	-15.5	
SCH J16092137-21393452	18.71	16.96	14.98	11.98	11.38	11.02	2.25	1.43	0.92	M5.5	-24.5	
SCH J16093018-20595409 <sup>j</sup>		19.41	17.30	13.99	13.35	12.98	2.59	1.53	0.89	M6	-11.1	
SCH J16093707-20525337	19.50	17.80	15.86	12.90	12.25	11.97	2.28	1.33	0.91	M4.75	-5.7	
SCH J16095217-21362826	20.24	18.33	16.05	12.56	11.96	11.56	2.66	1.76	0.94	M7	-26.2	
SCH J16095307-19481704		18.12	16.00	12.80	12.16	11.76	2.58	1.60	0.91	M6	-21.7	
SCH J16095695-22120300		18.72	16.49	13.62	13.03	12.66	2.64	1.53	0.90	M5.5	-8.9	
SCH J16095991-21554293 <sup>j</sup>		19.84	17.50	14.30	13.64	13.30	2.49	1.57	0.89	M6.5	-17.4	
SCH J16100129-21522466 <sup>b</sup>	19.75			12.63	12.06	11.70	2.53	1.55	0.91	M5.5	-12.0	
SCH J16100541-19193636		20.75	18.13	14.21	13.43	12.70	2.55	1.68	0.94	M6	-49.8	DENIS-P J161005.4-191936/M7 <sup>e</sup>
SCH J16100751-18105666		18.34	16.06	12.74	12.15	11.75	2.82	1.74	0.90	M6	-15.9	DENIS-P J161007.5-181056/M6 <sup>e</sup>
SCH J16101190-21015540	20.24	18.80	16.77	13.78	12.99	12.57	2.41	1.54	0.91	M5.5	-14.6	
SCH J16102990-24035024	18.97	17.42	15.59	12.92	12.33	12.01				M4.5	-10.0	
SCH J16103525-20291714	19.53	17.77	15.77	12.69	12.04	11.71	2.25	1.37	0.91	M5	-12.5	

Table 1—Continued

ID <sup>a</sup>	g	r	i	J <sup>c</sup>	H <sup>c</sup>	K <sub>S</sub> <sup>c</sup>	TiO-7140	TiO-8465	Na-8195	SpType <sup>d</sup>	W(H $\alpha$ ) [ $\text{\AA}$ ]	Other identification/SpType
SCH J16103876-18292353 <sup>j</sup>		19.87	17.63	13.96	13.16	12.64	2.29	1.57	0.96	M6	-80.3	
SCH J16104635-18405996	19.35	17.64	15.56	12.70	11.81	11.26	1.97	1.25	0.93	M4.5	-8.8	[PBB2002] USco J161046.3-184059/M4 <sup>f</sup>
SCH J16105500-21261422	19.71	18.19	16.03	12.77	12.10	11.77	2.59	1.59	0.90	M6	-27	
SCH J16105727-23595416	18.68	17.31	15.57	12.86	12.21	11.91				M4	-7.4	
SCH J16110144-19244914		18.44	16.43	13.35	12.71	12.36	2.27	1.39	0.90	M5	-9.3	
SCH J16110739-22285027	19.26	17.64	15.44	12.31	11.72	11.32	2.29	1.54	0.92	M6.25	-139.1	
SCH J16111711-22171749 <sup>j</sup>		20.37	17.97	14.34	13.73	13.25	2.68	1.82	0.94	M7.5	-20.8	
SCH J16112629-23400611		18.33	16.42	13.44	12.82	12.47	2.32	1.49	0.90	M5.5	-7.1	
SCH J16112959-19002921 <sup>j</sup>		19.76	17.35	13.67	12.90	12.44	2.49	1.68	0.94	M6	-20.4	
SCH J16114735-22420649		18.46	16.41	13.49	12.82	12.53	2.33	1.37	0.89	M5	-13.1	
SCH J16115737-22150691		18.75	16.70	13.73	13.10	12.73	2.26	1.39	0.90	M5	-8.6	
SCH J16121044-19322708	19.03	17.19	15.30	12.23	11.59	11.23	2.31	1.38	0.92	M5	-12.8	
SCH J16121188-20472698 <sup>j</sup>		19.39	17.09	13.66	13.02	12.60	2.69	1.77	0.93	M6.5	-8.1	
SCH J16122764-24064850	19.54	17.85	15.88	12.89	12.29	11.93				M7	-13.5	
SCH J16123459-24583447	18.37	16.87	14.83	11.94	11.36	11.04	2.26	1.36	0.91	M4.75	-13.5	
SCH J16123758-23492340 <sup>j</sup>		19.10	17.00	13.93	13.28	12.91	2.47	1.51	0.87	M6	-15.8	
SCH J16124506-23053043		18.70	16.52	13.48	12.87	12.46	2.48	1.43	0.87	M5.5	-9.8	
SCH J16124692-23384086 <sup>j</sup>		19.25	16.98	13.65	13.02	12.62	2.66	1.70	0.90	M6	-14.7	
SCH J16125723-24280145		17.46	15.68	12.93	12.28	11.95				M4	-11.8	
SCH J16130306-19293234		18.85	16.75	13.45	12.76	12.35	2.60	1.54	0.92	M5.5	-7.3	
SCH J16130764-17035233		18.95	16.83	13.71	13.02	12.71	2.32	1.46	0.90	M5.5	-7.9	
SCH J16131212-23050329 <sup>j</sup>		19.87	17.43	14.05	13.44	13.00	2.62	1.73	0.90	M6.5	-13.4	
SCH J16131857-15293460	17.87	16.50	14.49	11.68	11.05	10.76	2.23	1.34	0.93	M4.75	-14.4	
SCH J16132576-17373542 <sup>j</sup>	17.98	16.48	14.83	12.32	11.69	11.40	1.72	1.14	0.91	M4	-5.3	
SCH J16132809-19245288	19.87	18.22	16.16	12.92	12.26	11.91	2.46	1.47	0.91	M6	-14.7	[PBB2002] USco J161328.0-192452/M5 <sup>f</sup>
SCH J16141351-22445788		16.76	15.02	12.37	11.72	11.42				M4	-5.4	
SCH J16141484-24270844		17.83	15.60	12.47	11.85	11.48				M7	-17.6	
SCH J16141974-24284053 <sup>j</sup>		19.46	17.13	13.81	13.15	12.76	2.59	1.61	0.88	M6	-16.4	
SCH J16143286-22421358		20.54	17.87	14.23	13.66	13.24	2.77	1.75	0.98	M6.5	-23.6	
SCH J16150524-24593542		17.70	15.58	12.55	11.90	11.48	2.01	1.40	0.92	M5	-38.4	
SCH J16151115-24201556 <sup>j</sup>		19.68	17.46	14.23	13.58	13.17	2.33	1.43	0.90	M6	-10.9	
SCH J16151360-23042637		20.35	18.18	14.81	14.19	13.91	2.69	1.75	0.87	M6.5	-35.9	
SCH J16153915-19170073	19.03	17.32	15.09	11.68	10.84	10.43	2.11	1.31	0.93	M4.75	-9.3	
SCH J16155508-24443677 <sup>j</sup>		19.18	16.81	13.39	12.74	12.28	2.48	1.66	0.93	M6	-15.8	
SCH J16162396-24083016	19.69	17.67	16.02	13.15	12.51	12.13				M5	-17.5	
SCH J16162599-21122315		19.42	17.34	14.26	13.63	13.30	2.35	1.38	0.89	M5	-11.3	DENIS-P J161624.0-240830/M5.5 <sup>e</sup>
SCH J16163504-20575551	19.04	17.26	15.29	12.22	11.63	11.29	2.38	1.47	0.91	M5.5	-17.6	
SCH J16164538-23334143		18.79	16.77	13.77	13.15	12.81	2.27	1.39	0.86	M5	-17.1	
SCH J16165160-20485398	18.13	16.49	14.78	12.11	11.43	11.13				M4	-5.0	
SCH J16171901-21371312		18.78	16.65	13.48	12.86	12.54	2.52	1.49	0.91	M5.5	-13.4	
SCH J16172504-23503799 <sup>j</sup>		19.40	17.20	13.74	13.01	12.63	2.25	1.44	0.87	M5	-12.0	
SCH J16173105-20504715		18.83	16.49	13.03	12.36	12.02				M7	-34.8	
SCH J16173238-20403653		20.83	18.18	14.34	13.68	13.19	2.60	1.70	0.92	M6	-24.6	
SCH J16173788-21191618	18.41	16.84	14.93	12.23	11.54	11.26				M4	-8.7	
SCH J16174368-21115536	20.36	18.67	17.04	14.47	13.68	13.35				M4	-4.7	
SCH J16174540-23533618 <sup>j</sup>		19.88	17.44	14.05	13.31	12.95	2.83	1.67	0.91	M6	-15.5	
SCH J16181201-24133263	19.29	17.77	15.70	12.69	11.93	11.59				M5	-21.7	
SCH J16181567-23470847		18.55	16.18	12.42	11.51	10.97	2.32	1.39	0.94	M5.5	-16.3	
SCH J16181601-24372688	18.54	16.75	14.70	11.67	10.92	10.59				M4	-16.1	
SCH J16181906-20284815	19.13	17.36	15.38	12.39	11.50	10.95	2.14	1.31	0.91	M4.75	-11.3	
SCH J16182501-23381068 <sup>j</sup>		19.50	17.19	13.72	12.88	12.44	2.06	1.32	0.91	M5	-9.2	

Table 1—Continued

ID <sup>a</sup>	g	r	i	J <sup>c</sup>	H <sup>c</sup>	K <sub>S</sub> <sup>c</sup>	TiO-7140	TiO-8465	Na-8195	SpType <sup>d</sup>	W(H $\alpha$ ) [ $\text{\AA}$ ]	Other identification/SpType
SCH J16183144-24195229 <sup>j</sup>		20.22	17.76	14.15	13.46	12.97	2.45	1.60	0.87	M6.5	-11.4	
SCH J16183620-24253332	18.36	16.60	14.75	12.03	11.31	10.95				M4	-7.5	
SCH J16185038-24243205		18.97	16.79	13.63	12.93	12.51	2.34	1.38	0.90	M5	-6.5	
SCH J16190473-23075283		18.50	16.30	13.00	12.34	11.98	2.36	1.47	0.91	M5.5	-12.1	
SCH J16191521-24172429	19.00	17.23	15.19	12.13	11.37	11.05				M4	-13.3	
SCH J16192994-24255414	18.55	16.41	14.53	11.53	10.63	10.22				M4	-6.5	
SCH J16193976-21453527		18.47	16.40	13.22	12.53	12.11	2.10	1.66	0.93	M6	-36.5	DENIS-P J161939.8-214535/M7 <sup>e</sup>
SCH J16200756-23591522 <sup>j</sup>		19.14	16.75	13.21	12.48	12.05	2.49	1.58	0.92	M6	-24.2	
SCH J16201318-24250155		17.96	16.21	13.77	13.20	12.86				M4	-15.0	
SCH J16202127-21202923 <sup>j</sup>		19.14	16.61	13.39	12.74	12.40	2.61	1.62	0.89	M6	-23.9	
SCH J16202523-23160347 <sup>j</sup>		19.47	17.59	14.37	13.68	13.23	2.20	1.53	0.88	M5.5	-9.5	
SCH J16211564-24361173		15.86	14.50	12.44	11.81	11.59				M3.5	-5.0	
SCH J16211922-24255250		17.99	15.73	12.17	11.18	10.67				M4	-8.7	
SCH J16212490-24261446		18.24	16.14	12.87	11.86	11.41				M3.5	-6.8	
SCH J16213591-23550341 <sup>j</sup>		20.23	17.67	13.94	13.19	12.73	2.38	1.69	0.90	M6	-19.9	
SCH J16221577-23134936 <sup>j</sup>		18.87	16.80	13.71	13.14	12.80	2.52	1.55	0.87	M6	-9.2	
SCH J16222156-22173094 <sup>j</sup>		18.63	16.52	13.74	13.09	12.61	2.00	1.36	0.92	M5	-60.3	
SCH J16224384-19510575 <sup>j</sup>		17.54	15.88	12.35	11.61	11.15	2.42	2.13	0.98	M8	-62.1	
SCH J16235158-23172740 <sup>j</sup>		19.86	17.40	13.55	12.89	12.41	2.82	2.16	0.96	M8	-76.8	
SCH J16235474-24383211 <sup>j</sup>		19.77	17.21	13.31	12.49	11.92	2.34	1.61	0.95	M6	-12.8	
SCH J16252862-16585055 <sup>j</sup>		19.95	17.47	13.67	13.01	12.62	2.66	1.94	0.94	M8	-23.3	
SCH J16252968-22145448 <sup>j</sup>		18.64	16.40	13.19	12.49	12.11	2.25	1.41	0.94	M5	-16.2	
SCH J16253671-22242887 <sup>j</sup>		19.46	16.97	13.53	12.83	12.45	2.64	1.76	0.93	M7	-11.6	
SCH J16254319-22300300 <sup>j</sup>	19.35	17.22	15.84	13.02	12.40	12.09	2.19	1.37	0.90	M5	-9.2	
SCH J16255064-21554577		19.28	17.20	14.26	13.62	13.27	2.36	1.35	0.85	M4.75	-8.9	
SCH J16260630-23340375		19.31	16.85	13.14	12.27	11.75	2.28	1.41	0.93	M5.5	-5.4	
SCH J16263026-23365552 <sup>j</sup>		19.51	17.48	13.75	12.82	12.21	2.51	1.69	0.94	M6	-32.1	
SCH J16265619-22135224 <sup>j</sup>		19.14	16.76	13.48	12.83	12.41	2.71	1.67	0.90	M6	-28.4	
SCH J16270940-21484591		18.39	16.29	12.97	12.15	11.71	1.85	1.27	0.92	M4.5	-11.1	
SCH J16274801-24571371 <sup>j</sup>		19.87	17.31	13.54	12.65	12.11	2.20	1.42	0.91	M5	-22.0	
SCH J16281810-24283619		19.19	16.55	12.69	11.81	11.29	2.43	1.49	0.93	M6	-20.1	BKLT J162818-242836 <sup>g</sup>
SCH J16284706-24281413		18.71	16.59	13.24	12.53	11.95	2.16	1.72	0.94	M6	-182.7	BKLT J162847-242814 <sup>g</sup>
SCH J16292211-17420937	19.23	17.48	15.46	12.58	12.02	11.72	2.17	1.36	0.88	M4.75	-13.0	
SCH J16293625-24565325		18.66	16.43	13.43	12.85	12.48	2.90	1.59	0.86	M6	-41.2	
SCH J16293664-17084094	18.39	16.74	14.82	12.01	11.31	11.01	2.16	1.31	0.91	M4.75	-11.3	
SCH J16293934-16145647	17.35	15.90	14.51	12.19	11.49	11.19				M3	-3.1	
SCH J16294877-21370914 <sup>j</sup>	19.13	17.38	15.45	12.52	11.86	11.52	2.16	1.34	0.92	M5	-9.2	
SCH J16302675-23590905		18.26	16.02	12.61	11.93	11.47	2.39	1.64	0.96	M6	-34.7	
SCH J16303392-24280657		16.67	14.67	11.62	10.76	10.36				M4	-5.3	
SCH J16305349-24245439		17.51	15.51	12.27	11.46	11.04	2.21	1.41	0.97	M5.5	-34.8	
SCH J16310241-24084335		16.70	14.67	11.96	11.24	10.78				M5	-13.5	WSB 68 <sup>i</sup>
SCH J16324224-23165644		16.77	14.70	11.76	11.17	10.87	2.60	1.48	0.87	M5.5	-12.9	
SCH J16324726-20593771 <sup>j</sup>		18.49	16.55	13.45	12.85	12.47	2.39	1.50	0.91	M6	-25.2	

<sup>a</sup>IDs given in J2000 coordinates.<sup>b</sup>Two targets observed during the first spectroscopic observing run before the final photometric calibrations were finished do not have calibrated  $r$ ,  $i$  magnitudes.<sup>c</sup>Near-infrared photometry taken from 2MASS.<sup>d</sup>Spectral type errors are  $\pm 0.5$  for M subclasses.

<sup>e</sup>Martín et al. (2004).

<sup>f</sup>Preibisch et al. (2002).

<sup>g</sup>Barsony et al (1997).

<sup>h</sup>Ardila et al (2000).

<sup>i</sup>Wilking et al. (1987).

<sup>j</sup>Star identified as a member of USco in Paper I.

Table 2. Derived quantities for new USco members

ID	$\log(T_{eff}/K)$	$\log(L/L_{\odot})$	$\log(age/yr)^a$	$M/M_{\odot}^a$
SCH15560497-21064632	3.41	-2.17	5.46	0.03
SCH15561978-24232936	3.47	-1.87	7.10	0.12
SCH15574757-24441236	3.49	-1.69	7.09	0.16
SCH15582337-21515908	3.47	-1.39	6.54	0.13
SCH15582566-18260865	3.44	-1.65	6.41	0.06
SCH15583162-24025411	3.47	-1.76	7.00	0.12
SCH15584812-21413426	3.45	-1.95	6.75	0.06
SCH15594802-22271650	3.40	-2.27	5.35	0.02
SCH15595868-18365205	3.45	-1.88	6.71	0.06
SCH16002669-20563190	3.47	-1.95	7.17	0.11
SCH16014156-21113855	3.49	-1.52	6.88	0.16
SCH16014768-24410152	3.46	-2.11	7.06	0.07
SCH16024143-22484204	3.45	-1.76	6.64	0.07
SCH16024576-23045102	3.46	-1.52	6.61	0.11
SCH16033470-18293060	3.46	-1.48	6.57	0.11
SCH16034029-23352386	3.49	-1.40	6.70	0.17
SCH16035651-23572517	3.47	-1.99	7.21	0.11
SCH16040453-23463795	3.49	-1.13	6.35	0.16
SCH16044303-23182620	3.42	-2.12	5.96	0.03
SCH16051829-17562092	3.49	-1.12	6.34	0.16
SCH16053077-22462016	3.44	-2.10	6.75	0.04
SCH16054416-21550566	3.46	-1.30	6.42	0.12
SCH16060391-20564497	3.41	-2.02	5.44	0.03
SCH16072239-20115852	3.45	-1.57	6.54	0.08
SCH16072640-21441727	3.44	-2.42	6.94	0.03
SCH16075565-24432714	3.45	-2.00	6.78	0.06
SCH16075850-20394890	3.44	-1.99	6.68	0.04
SCH16081081-22294303	3.46	-1.58	6.66	0.11
SCH16083646-24453053	3.50	-1.10	6.41	0.18
SCH16083658-18024994	3.42	-1.71	5.64	0.05
SCH16084058-22255726	3.49	-2.14	7.60	0.13
SCH16084170-18561077	3.44	-1.45	6.09	0.07
SCH16085870-24493641	3.49	-1.40	6.71	0.17
SCH16090451-22245259	3.41	-1.78	5.39	0.04
SCH16090511-24262843	3.49	-1.21	6.45	0.16
SCH16090771-23395430	3.46	-1.35	6.46	0.12
SCH16090883-22174699	3.46	-1.71	6.76	0.10
SCH16091837-20073523	3.40	-1.81	5.01	0.02
SCH16092137-21393452	3.45	-1.37	6.39	0.10
SCH16093018-20595409	3.44	-2.15	6.77	0.04
SCH16093707-20525337	3.47	-1.66	6.81	0.12
SCH16095217-21362826	3.41	-1.63	5.36	0.04
SCH16095307-19481704	3.44	-1.68	6.43	0.06
SCH16095695-22120300	3.45	-2.03	6.80	0.06
SCH16095991-21554293	3.42	-2.27	6.16	0.03
SCH16100129-21522466	3.45	-1.64	6.57	0.08

Table 2—Continued

ID	$\log(T_{eff}/\text{K})$	$\log(L/L_{\odot})$	$\log(\text{age}/\text{yr})^{\text{a}}$	$M/M_{\odot}^{\text{a}}$
SCH16100541-19193636	3.44	-2.10	6.74	0.04
SCH16100751-18105666	3.44	-1.69	6.44	0.06
SCH16101190-21015540	3.45	-1.91	6.73	0.06
SCH16102990-24035024	3.47	-1.72	6.96	0.13
SCH16103525-20291714	3.46	-1.59	6.66	0.11
SCH16103876-18292353	3.44	-1.99	6.68	0.04
SCH16104635-18405996	3.47	-1.34	6.53	0.14
SCH16105500-21261422	3.44	-1.63	6.40	0.06
SCH16105727-23595416	3.49	-1.62	7.01	0.16
SCH16110144-19244914	3.46	-1.86	6.88	0.09
SCH16110739-22285027	3.43	-1.52	5.75	0.06
SCH16111711-22171749	3.40	-2.35	5.38	0.02
SCH16112629-23400611	3.45	-1.93	6.74	0.06
SCH16112959-19002921	3.44	-1.90	6.61	0.05
SCH16114735-22420649	3.46	-1.88	6.90	0.09
SCH16115737-22150691	3.46	-2.02	7.00	0.08
SCH16121044-19322708	3.46	-1.41	6.51	0.12
SCH16121188-20472698	3.42	-2.04	5.87	0.03
SCH16122764-24064850	3.41	-1.76	5.39	0.04
SCH16123459-24583447	3.47	-1.34	6.49	0.13
SCH16123758-23492340	3.44	-2.11	6.75	0.04
SCH16124506-23053043	3.45	-1.95	6.75	0.06
SCH16124692-23384086	3.44	-2.02	6.70	0.04
SCH16125723-24280145	3.49	-1.65	7.04	0.16
SCH16130306-19293234	3.45	-1.87	6.70	0.06
SCH16130764-17035233	3.45	-1.97	6.76	0.06
SCH16131212-23050329	3.42	-2.22	6.09	0.03
SCH16131857-15293460	3.47	-1.18	6.34	0.13
SCH16132576-17373542	3.49	-1.43	6.74	0.17
SCH16132809-19245288	3.44	-1.70	6.45	0.06
SCH16141351-22445788	3.49	-1.42	6.74	0.17
SCH16141484-24270844	3.41	-1.59	5.35	0.04
SCH16141974-24284053	3.44	-2.06	6.72	0.04
SCH16143286-22421358	3.42	-2.29	6.18	0.03
SCH16150524-24593542	3.46	-1.52	6.61	0.11
SCH16151115-24201556	3.44	-2.24	6.82	0.04
SCH16151360-23042637	3.42	-2.51	6.89	0.03
SCH16153915-19170073	3.47	-0.99	6.08	0.13
SCH16155508-24443677	3.44	-1.90	6.61	0.05
SCH16162396-24083016	3.46	-1.77	6.81	0.09
SCH16162599-21122315	3.46	-2.23	7.16	0.07
SCH16163504-20575551	3.45	-1.47	6.48	0.09
SCH16164538-23334143	3.46	-2.05	7.01	0.08
SCH16165160-20485398	3.49	-1.29	6.56	0.16
SCH16171901-21371312	3.45	-1.94	6.75	0.06
SCH16172504-23503799	3.46	-1.93	6.93	0.08

Table 2—Continued

ID	$\log(T_{eff}/K)$	$\log(L/L_{\odot})$	$\log(age/yr)^a$	$M/M_{\odot}^a$
SCH16173105-20504715	3.41	-1.78	5.39	0.04
SCH16173238-20403653	3.44	-2.27	6.84	0.04
SCH16173788-21191618	3.49	-1.33	6.61	0.16
SCH16174368-21115536	3.49	-2.13	7.59	0.13
SCH16174540-23533618	3.44	-2.08	6.73	0.04
SCH16181201-24133263	3.46	-1.47	6.57	0.11
SCH16181567-23470847	3.45	-1.24	6.26	0.10
SCH16181601-24372688	3.49	-1.05	6.26	0.16
SCH16181906-20284815	3.47	-1.22	6.37	0.13
SCH16182501-23381068	3.46	-1.81	6.85	0.09
SCH16183144-24195229	3.42	-2.18	6.04	0.03
SCH16183620-24253332	3.49	-1.23	6.47	0.16
SCH16185038-24243205	3.46	-1.91	6.92	0.08
SCH16190473-23075283	3.45	-1.72	6.62	0.07
SCH16191521-24172429	3.49	-1.22	6.47	0.16
SCH16192994-24255414	3.49	-0.85	6.05	0.15
SCH16193976-21453527	3.44	-1.80	6.53	0.05
SCH16200756-23591522	3.44	-1.75	6.49	0.05
SCH16201318-24250155	3.49	-2.06	7.52	0.14
SCH16202127-21202923	3.44	-1.90	6.61	0.05
SCH16202523-23160347	3.45	-2.23	6.94	0.05
SCH16211564-24361173	3.50	-1.47	6.93	0.19
SCH16211922-24255250	3.49	-1.01	6.22	0.16
SCH16212490-24261446	3.50	-1.27	6.64	0.19
SCH16213591-23550341	3.44	-2.02	6.70	0.04
SCH16221577-23134936	3.44	-2.08	6.73	0.04
SCH16222156-22173094	3.46	-2.00	6.98	0.08
SCH16224384-19510575	3.39	-1.48	–	0.04
SCH16235158-23172740	3.39	-2.03	–	0.02
SCH16235474-24383211	3.44	-1.70	6.45	0.06
SCH16252862-16585055	3.39	-2.08	–	0.02
SCH16252968-22145448	3.46	-1.73	6.78	0.10
SCH16253671-22242887	3.41	-1.95	5.42	0.03
SCH16254319-22300300	3.46	-1.74	6.79	0.10
SCH16255064-21554577	3.47	-2.21	7.28	0.08
SCH16260630-23340375	3.45	-1.56	6.53	0.08
SCH16263026-23365552	3.44	-1.77	6.51	0.05
SCH16265619-22135224	3.44	-1.94	6.64	0.05
SCH16270940-21484591	3.47	-1.52	6.73	0.14
SCH16274801-24571371	3.46	-1.69	6.75	0.10
SCH16281810-24283619	3.44	-1.39	5.95	0.08
SCH16284706-24281413	3.44	-1.78	6.51	0.05
SCH16292211-17420937	3.47	-1.60	6.75	0.12
SCH16293625-24565325	3.44	-1.97	6.66	0.05
SCH16293664-17084094	3.47	-1.26	6.41	0.13
SCH16293934-16145647	3.51	-1.29	6.79	0.22

Table 2—Continued

ID	$\log(T_{eff}/\text{K})$	$\log(L/L_{\odot})$	$\log(\text{age}/\text{yr})^{\text{a}}$	$M/M_{\odot}^{\text{a}}$
SCH16294877-21370914	3.46	-1.51	6.60	0.11
SCH16302675-23590905	3.44	-1.56	6.34	0.07
SCH16303392-24280657	3.49	-0.92	6.13	0.15
SCH16305349-24245439	3.45	-1.27	6.31	0.10
SCH16310241-24084335	3.46	-1.22	6.35	0.12
SCH16324224-23165644	3.45	-1.29	6.33	0.10
SCH16324726-20593771	3.44	-1.97	6.66	0.04

<sup>a</sup>Masses and ages derived from the model tracks and isochrones of DM97.

Table 3. Measured Quantities for Spectroscopically Confirmed Field Dwarfs

ID <sup>a</sup>	g	r	i	J <sup>b</sup>	H <sup>b</sup>	K <sub>S</sub> <sup>b</sup>
SCH J15561830-24183193		17.10	15.59	13.25	12.56	12.28
SCH J15563309-18074323		20.29	17.67	14.18	13.61	13.13
SCH J15564167-24174525		17.04	15.45	13.14	12.55	12.29
SCH J15572004-24462048	18.89	17.41	15.76	13.35	12.74	12.46
SCH J15582384-15310335		16.64	14.88	12.36	11.79	11.52
SCH J15591269-17253418	20.04	18.55	16.81	14.15	13.49	13.12
SCH J15592588-18072310		18.77	16.82	13.98	13.32	12.95
SCH J15593963-17461084	19.42	17.84	16.22	13.77	13.02	12.73
SCH J16005404-24143743		20.51	18.25	15.07	14.62	14.11
SCH J16010703-20591882	18.37	16.86	15.35	12.94	12.41	12.12
SCH J16021574-23435806	17.28	15.87	14.43	12.17	11.48	11.25
SCH J16030530-24090255		15.89	14.47	12.27	11.76	11.49
SCH J16032871-21583609		19.33	17.54	14.62	13.96	13.59
SCH J16035236-23564424	17.93	16.38	14.96	12.67	12.09	11.78
SCH J16070403-14352587	17.85	16.40	14.67	12.28	11.73	11.41
SCH J16073811-15120357		18.84	16.36	12.95	12.31	11.92
SCH J16080516-24334024	18.17	16.81	15.26	13.02	12.44	12.15
SCH J16084199-22165277	18.42	16.86	15.18	12.98	12.43	12.16
SCH J16084729-19553026		20.08	18.04	15.05	14.33	13.94
SCH J16091254-21582262		19.12	17.23	14.39	13.77	13.49
SCH J16091802-19213678		19.64	17.51	14.57	13.88	13.57
SCH J16092099-16113026		19.08	17.05	14.10	13.47	13.18
SCH J16092940-23431209		19.57	17.54	14.20	13.57	13.21
SCH J16103948-19170814	20.73	18.84	16.43	13.30	12.63	12.25
SCH J16104971-22223447	19.34	17.82	16.17	13.79	13.12	12.82
SCH J16111908-23192035		17.72	15.79	11.69	10.98	10.69
SCH J16113079-20272907	18.74	17.12	15.68	13.29	12.60	12.34
SCH J16113396-16330396		24.25	17.64	13.92	13.20	12.93
SCH J16122878-19590143		21.03	18.68	15.20	14.54	14.10
SCH J16123730-17353318		19.58	17.44	14.47	13.85	13.51
SCH J16123986-19213903		19.53	17.49	14.52	13.86	13.43
SCH J16124229-16344528		16.50	15.29	12.98	12.23	11.97
SCH J16124698-23145895	16.81	15.41	14.11	12.07	11.49	11.23

Table 3—Continued

ID <sup>a</sup>	g	r	i	J <sup>b</sup>	H <sup>b</sup>	K <sub>S</sub> <sup>b</sup>
SCH J16135278-19221088	20.01	19.76	17.57	14.42	13.88	13.49
SCH J16140298-19504728		18.64	16.56	13.57	12.95	12.60
SCH J16143180-22480187	16.75	15.37	14.16	12.04	11.43	11.14
SCH J16144750-22460541	17.11	15.64	14.42	12.23	11.54	11.30
SCH J16152005-23335510		17.85	15.79	12.96	12.35	11.92
SCH J16161043-21480822		19.68	17.35	14.33	13.74	13.48
SCH J16161911-19220165		20.66	18.60	15.41	14.57	14.10
SCH J16171520-20553873	17.45	15.91	14.71	12.69	12.02	11.70
SCH J16171826-20423558	20.23	18.45	16.81	14.11	13.37	12.98
SCH J16174019-22230511		20.97	18.38	15.11	14.60	14.20
SCH J16175769-24040201		18.93	17.18	14.58	13.87	13.49
SCH J16180572-20552860	19.78	18.11	16.58	14.16	13.42	13.08
SCH J16192530-23470717		19.07	17.10	14.01	13.17	12.75
SCH J16193687-24480420	15.70	14.42	13.62	11.67	11.02	10.76
SCH J16194753-24434983	19.99	18.16	16.43	13.60	12.64	12.25
SCH J16194826-24291678	16.60	15.10	14.15	11.90	11.18	10.92
SCH J16194994-24290920		18.76	16.31	12.64	11.77	11.35
SCH J16195935-24362497	15.96	14.72	13.87	11.88	11.19	11.02
SCH J16200923-20283157		20.63	18.48	15.09	14.32	13.89
SCH J16201032-24474958	15.79	14.46	13.65	11.70	10.98	10.73
SCH J16202226-24460539		19.49	17.28	14.32	13.74	13.38
SCH J16202731-24282582		17.20	15.89	13.20	12.29	11.91
SCH J16202753-14082840		16.53	14.78	12.22	11.56	11.27
SCH J16203331-24464616		19.76	17.73	14.70	13.96	13.53
SCH J16205818-24380368	16.49	15.12	14.23	12.10	11.39	11.14
SCH J16214647-21424605		20.88	18.31	14.97	14.42	14.17
SCH J16220181-22493721	19.38	17.51	15.60	12.39	11.56	11.16
SCH J16223315-14422746		18.19	16.23	13.49	12.84	12.51
SCH J16230250-19472068		18.28	16.73	13.88	12.90	12.45
SCH J16231687-20303292		20.26	18.18	14.85	13.99	13.56
SCH J16235601-23583999		19.61	17.44	14.53	14.01	13.57
SCH J16242790-20070221		20.69	18.35	14.98	14.36	14.00
SCH J16242880-20385513		19.49	17.66	14.58	13.77	13.31

Table 3—Continued

ID <sup>a</sup>	g	r	i	J <sup>b</sup>	H <sup>b</sup>	K <sub>S</sub> <sup>b</sup>
SCH J16245227-17024443		19.79	17.87	14.76	13.98	13.58
SCH J16252609-15401969		17.93	16.33	13.67	12.94	12.52
SCH J16253844-21590488		19.49	17.41	14.61	14.06	13.68
SCH J16255124-21553824		16.30	14.76	12.34	11.60	11.31
SCH J16260856-22120485		19.82	17.82	14.90	14.20	13.70
SCH J16261170-18070142		18.87	16.91	14.22	13.58	13.24
SCH J16261663-20425464		20.41	18.36	15.22	14.50	14.04
SCH J16270959-16204810	19.95	17.88	16.34	13.55	12.72	12.28
SCH J16280542-14053116		19.31	17.29	14.50	13.78	13.39
SCH J16280572-15574487		15.97	14.49	12.28	11.66	11.41
SCH J16280816-15570530		15.65	14.22	12.05	11.46	11.19
SCH J16282246-18584895		19.54	17.40	14.32	13.72	13.36
SCH J16283942-16140460	18.77	16.83	15.58	13.15	12.33	11.98
SCH J16284798-16023117	16.30	14.80	13.91	11.70	10.97	10.68
SCH J16290665-22464968		19.22	17.22	14.03	13.19	12.77
SCH J16291911-16410107	19.07	17.31	15.62	12.85	12.12	11.76
SCH J16293713-19172311		21.41	18.87	15.41	14.75	14.25
SCH J16300989-24243554		14.70	13.92	11.92	11.20	10.95
SCH J16301483-22435159		19.40	17.58	14.57	13.71	13.20
SCH J16301682-15574807		18.63	16.63	13.59	12.86	12.53
SCH J16303166-16093250		18.12	16.22	13.38	12.69	12.37
SCH J16310033-24061395		19.78	16.91	14.17	13.41	13.12
SCH J16310498-21591346		19.54	17.37	14.48	13.84	13.50
SCH J16311682-18361254		20.35	18.01	15.06	14.32	13.82
SCH J16311916-23375496		14.80	13.92	11.60	10.82	10.52
SCH J16314540-24272121		15.12	13.95	11.11	10.14	9.68
SCH J16320046-22151654		17.87	15.69	12.63	11.79	11.38
SCH J16323549-24235273		15.97	14.54	12.38	11.83	11.59
SCH J16325225-21075439		15.31	14.15	12.19	11.61	11.33
SCH J16325602-16582835		16.45	14.75	12.26	11.76	11.44
SCH J16333539-21202087		19.97	17.71	14.99	14.19	13.82
SCH J16343354-18285082		19.93	17.92	14.92	14.18	13.80

<sup>a</sup>IDs given in J2000 coordinates.

<sup>b</sup>Near-infrared photometry taken from 2MASS.